SPARSE SENSOR ARRAY DESIGN VIA CONSTRAINED OPTIMIZATION

A THESIS SUBMITTED TO
THE GRADUATE SCHOOL OF NATURAL AND APPLIED SCIENCES
OF
MIDDLE EAST TECHNICAL UNIVERSITY

BY

GÖKHAN GÖK

IN PARTIAL FULFILLMENT OF THE REQUIREMENTS
FOR
THE DEGREE OF MASTER OF SCIENCE
IN
ELECTRICAL AND ELECTRONICS ENGINEERING

SEPTEMBER 2013

Approval of the thesis:

SPARSE SENSOR ARRAY DESIGN VIA CONSTRAINED OPTIMIZATION

submitted by **GÖKHAN GÖK** in partial fulfillment of the requirements for the degree of **Master of Science in Electrical and Electronics Engineering Department, Middle East Technical University** by,

Prof. Dr. Canan Özgen
Dean, Graduate School of **Natural and Applied Sciences** _____

Prof. Dr. Gönül Turhan Sayan
Head of Department, **Electrical and Electronics Engineering** _____

Prof. Dr. T. Engin Tuncer
Supervisor, **Electrical and Electronics Engineering Dept., METU** _____

Examining Committee Members:

Associate Prof. Dr. Ali Özgür Yılmaz
Electrical and Electronics Engineering Dept., METU _____

Prof. Dr. T. Engin Tuncer
Electrical and Electronics Engineering Dept., METU _____

Assoc. Prof. Dr. Çağatay Candan
Electrical and Electronics Engineering Dept., METU _____

Asst. Prof. Dr. Umut Orguner
Electrical and Electronics Engineering Dept., METU _____

Aydın Bayri, M.Sc.
Aselsan Inc. _____

Date: _____

I hereby declare that all information in this document has been obtained and presented in accordance with academic rules and ethical conduct. I also declare that, as required by these rules and conduct, I have fully cited and referenced all material and results that are not original to this work.

Name, Last Name: GÖKHAN GÖK

Signature :

ABSTRACT

SPARSE SENSOR ARRAY DESIGN VIA CONSTRAINED OPTIMIZATION

GÖK, Gökhan
M.S., Department of Electrical and Electronics Engineering
Supervisor : Prof. Dr. T. Engin Tuncer

September 2013, 66 pages

In direction finding applications, sparse array design is an important problem. Sparse arrays are desired when the number of receivers are limited or when sensor size is large compared to half wavelength. When the sparse array design with inter element spacing greater than half wavelength is considered, ambiguity should be avoided as much as possible. The design should generate array patterns without grating lobes.

In this thesis, a similarity measure related to ambiguity probability is used to design sparse arrays. This measure is also related to the DOA estimation accuracy and resolution. The design problem setting is cast in a form suitable for linear binary programming. The design criteria includes worst-case ambiguity probability, DOA accuracy, sensor dimensions and maximum array aperture. The proposed approach is used to design one and two dimensional sparse arrays. It is shown that the proposed approach is effective and presents certain advantages compared to the alternative methods.

Keywords: Sparse Arrays, Ambiguity Problem, Binary Programming

ÖZ

KISITLANMIŞ EN İYİLEME İLE SEYREK DİZİ TASARIMI

GÖK, Gökhan
Yüksek Lisans, Elektrik ve Elektronik Mühendisliği Bölümü
Tez Yöneticisi : Prof. Dr. T. Engin Tuncer

Eylül 2013 , 66 sayfa

Yön Bulma uygulamalarında seyrek dizi tasarımı önemli bir problemdir. Almaç sayıları yetersiz olduğunda veya sezici boyutları yarım dalga boyundan büyük olduğu durumlarda seyrek dizilere ihtiyaç duyulmaktadır. Elemanlar arası uzaklığın yarım dalga boyundan büyük olduğu durumlarda belirsizliklerden mümkün olduğunca kaçınılmalıdır. Tasarlanan diziler yüksek yan lobları olmayan örüntüler oluşturmalıdır.

Bu tezde, seyrek diziler oluşturmak için belirsizlik olasılığı ile direk olarak ilgili olan bir benzerlik ölçütü kullanılmıştır. Bu benzerlik ölçütü geliş açısı kestirim doğruluğu ve çözünürlüğü ile de bağlantılıdır. Tasarım problemi doğrusal ikili değer programı biçimine getirilmiştir. Tasarım kriterleri, en kötü belirsizlik olasılığı, yön kestirim doğruluğu, sezici boyutları ve en büyük dizi boyutunu içermektedir. Önerilen yöntem kullanılarak bir ve iki boyutlu seyrek diziler tasarlanmıştır.Önerilen yaklaşımın etkili bir yöntem olduğu ve alternatif yöntemlere göre bazı avantajları olduğu gösterilmiştir.

Anahtar Kelimeler: Sparse Array, Belirsizlik Problemi,binary problemi

to my beloved cat and my family

ACKNOWLEDGMENTS

First and foremost, I would like to thank my supervisor Prof. T.Engin Tuncer for his exhaustless support and guidance throughout this period.

I am very grateful to Aselsan Inc. for providing me the opportunity and motivation to pursue my research. Also I would like to thank all my colleagues for their contributions. Especially, I would like to thank Y.Kemal Alp for his helpful discussions.

Finally, I would like to thank my family for their endless encouragement and support through my whole life.

TABLE OF CONTENTS

LIST OF TABLES

TABLES

LIST OF FIGURES

FIGURES

LIST OF ABBREVIATIONS

AOA	Angle of Arrival
DF	Direction Finding
DOA	Direction of Arrival
CRB	Cramer Rao Bound
BLP	Binary Linear Programm
SNR	Signal to Noise Ratio
MSE	Mean Square Error
MLE	Maximum Likelihood Estimation
RMSE	Root Mean Square Error
BW	Beamwidth

CHAPTER 1

INTRODUCTION

Direction Finding(DF) or Direction of Arrival(DOA) estimation can be stated as determining the incoming angle of a signal that is radiated by a distant emitter and it has numerous applications in variety of fields such as sonar, radar, communications, navigation or electronic warfare(EW). Signals coming from multiple sensors are received using multiple receivers and then processed in order to determine the angle-of-arrival(AOA) of incoming signals. There is a large DOA literature that explains how the processing should be done for best estimation performance in terms of different performance criterion like resolution or estimation variance. Array geometry has also a large impact on DOA estimation performance. Cramer-Rao bound(CRB) is directly determined by how the sensors are placed in the space[1][2].

Direction finding systems usually employ sensor arrays with unequal sensor spacings for various reasons. One of the main reason of using unequal sensor spacing in array designs is to have better estimation accuracy and resolution compared to equispaced counterparts with the same number of elements. It is well known that increasing the maximum aperture of a sensor array result in a better estimation accuracy and resolution. But in [3, 4], it is shown that for sensor spacing larger than $\frac{\lambda}{2}$, ambiguities might occur. In [5][6], ambiguity defined as producing large direction of arrival errors when two or more steering vectors are similar for widely spaced angles. In other words for different direction of arrivals, array might have same response at its output and these direction of arrivals cannot be distinguished from each other. Such arrays are said to be ambiguous. Difference between observation spaces of ambiguous and unambiguous array is conceptually illustrated in Fig. 1.1.

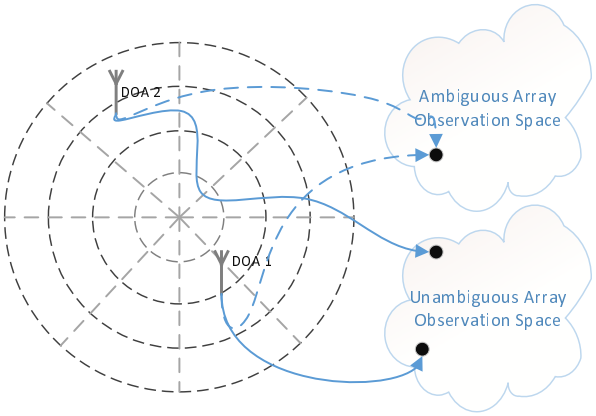

Figure 1.1: Observation Spaces of Ambiguous and Unambiguous Arrays

Accuracy is not the only reason for using arrays with large spacings. Sometimes sensors are so large that they cannot be positioned close to each other. For closely spaced sensors, performance might degrade due to the mutual couplings. Especially for wide-band systems, sensor sizes might be greater than one or even two wavelengths in the largest frequency of operation. So it is important to identify feasible sensor positions to have unambiguous array response for large array elements.

1.1 Scope and Contributions of the Thesis

In this thesis, we propose a new method for properly selecting sensor locations for ambiguity resolution. To do this, we first investigate the ambiguity phenomenon and find the relation between sensor array geometry, ambiguity probability and estimation performance. After that array design problem is modelled as a Binary Linear Program(BLP) and ambiguity constraints along with the accuracy requirements are used as the constraints of the problem. Although BLPs are known to be non-convex and NP hard, there are very powerful methods like branch-and-bound algorithm that finds the optimal solution by solving linear relaxations of the original problem. Details of these algorithms are not discussed in here as it is not in the scope of this thesis.

Contributions of the array design method proposed in this thesis are stated below.

- Sensor arrays with large baselines and worst case ambiguity probability limited

by a desired value can be designed with proposed approach. Design approach tries to find a sensor array geometry with minimum number of sensor that satisfy both worst case ambiguity probability and required DF accuracy. In most practical problems, number of receivers are limited and DOA estimation requirements are tight. In order to satisfy the accuracy requirements, sparse arrays with large baselines are needed.

- Especially for wide band sensor arrays, sensor sizes are large. In the proposed approach sensor dimensions are directly incorporated in the design procedure. They are modelled as linear constraints and added to the optimization problem.

- Maximum aperture of the array is also set as a design parameter. Especially for moving platforms, there is not always a large enough space for placement. These kind of requirements are handled by the proposed approach inherently.

- The proposed method is first proposed for linear array design and then it is shown that it can be used for arbitrary array geometries in 3D space. Most alternative approaches are limited to 1D space only.

To show the efficiency of the approach, in Chapter 5, we present some examples for both linear array for 1D DOA estimation and planar array for 2D DOA estimation. Results are supported with DOA accuracy simulations.

CHAPTER 2

BACKGROUND INFORMATION

2.1 Signal Model

The emphasis in this chapter will be on introducing the signal model for the output of the receiving sensor array. By using the given signal model, direction of arrival estimation problem is turned into a parameter estimation problem using the noisy snapshots of the sensor array. During the derivations two important assumptions will be made. First one is the narrowband assumption and it gives us the ability to write the output of each sensor as phase shifted copies of the emitter signal. Second assumption is the far field assumption and it simply lets us to write the propagation delay between sensors as a function of direction of arrival of the signal. For readability, we will begin by considering the single source case. Once the model for single source is established, general model for multiple source signals will be obtained just by using the superposition principle.

Now consider the scenario given in Fig. 2.1 with M sensors. ϕ is the azimuth angle measured from x-axis on xy plane and θ is the elevation angle measured from positive z-axis.

Let $s_p(t)$ denote the passband signal that would be received at the origin of the coordinate system given by

$$s_p(t) \triangleq \Re\{s(t)e^{j2\pi f_c t}\} \tag{2.1}$$

where $s(t)$ denotes the complex envelope and f_c is the carrier frequency.

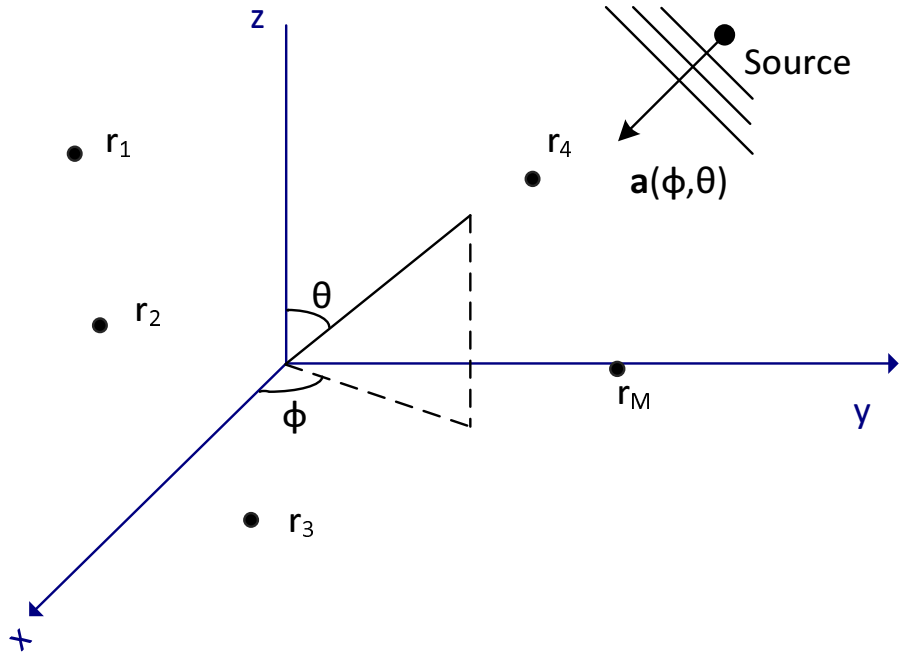

Figure 2.1: M Element Sensor Array and the Coordinate System

Signal received by the ith sensor is given by

$$s_{pi}(t) = s_p(t - \tau_i) = \Re\{s(t - \tau_i)e^{j2\pi f_c t}e^{-j2\pi f_c \tau_i}\} \tag{2.2}$$

where τ_i is the time delay needed for the wave to travel from origin to sensor $i.(i = 1, 2 \dots M)$. Let B denote the bandwidth of the emitter signal $s(t)$. If $B \ll \frac{1}{\tau_i}$ for all sensors then $s(t-\tau_i) \approx s(t)$. This assumption is known as the narrowband assumption. Using this assumption, output of the sensor i is given by

$$s_{pi}(t) = s_p(t - \tau_i) = \Re\{s(t)e^{j2\pi f_c t}e^{-j2\pi f_c \tau_i}\} \tag{2.3}$$

After demodulating the passband signals, the baseband signal measured from each sensor is given by

$$y_i(t) = s(t)e^{-j2\pi f_c \tau_i} + v(t) \tag{2.4}$$

where $v(t)$ denotes the additive noise term.

Notice that the signal received by each sensor is phase shifted by the delay amount τ_i. Using the far field assumption(planar wave assumption), delay term τ_i can be written

as a function of direction of arrival $\{\phi, \theta\}$ and sensor position (x_i, y_i, z_i).

$$\tau_i = \frac{\boldsymbol{r}_i^T \boldsymbol{u}}{c} \tag{2.5}$$

where

$$\boldsymbol{r}_i \triangleq [x_i \ y_i \ z_i]^T \tag{2.6}$$

$$\boldsymbol{u} \triangleq [cos\phi sin\theta \ sin\phi sin\theta \ cos\theta]^T \tag{2.7}$$

and c is the propagation velocity of the impinging waveform(for example, the speed of light in the case of electromagnetic waves). In Fig. 2.2, planar wave assumption is illustrated for a linear array positioned on x-axis.

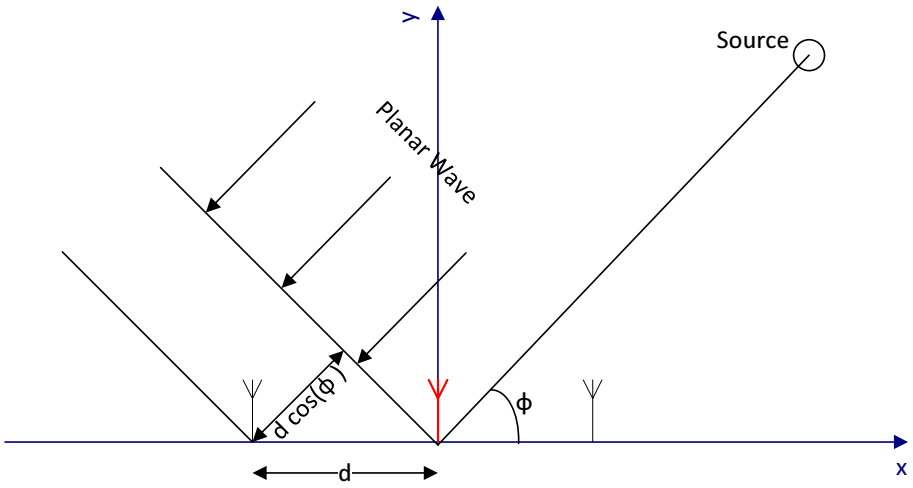

Figure 2.2: Planar Wave Assumption for Linear Array

Substituting the Eq. 2.5 into Eq. 2.4, we get

$$y_i(t) = s(t)e^{-j2\pi \frac{\boldsymbol{r}_i^T \boldsymbol{u}}{\lambda}} + v(t) \tag{2.8}$$

where λ denotes the signal wavelength which is the distance travelled by the waveform in one period.

$$\lambda = \frac{c}{f_c} \tag{2.9}$$

For signal source case, signal received by the array can be written in vector form as

below.

$$\boldsymbol{y}(t) \triangleq \begin{bmatrix} y_1(t) \\ y_2(t) \\ \vdots \\ y_M(t) \end{bmatrix} = \boldsymbol{a}(\phi,\theta)s(t) + \boldsymbol{v}(t) \tag{2.10}$$

The vector $\boldsymbol{a}(\phi,\theta)$ in Eq. 2.10 is referred as the **array manifold vector** and incorporates all of the spatial characteristics of the array. Array manifold vector can be given by

$$\boldsymbol{a}(\phi,\theta) \triangleq \begin{bmatrix} e^{-j2\pi\frac{\boldsymbol{r}_1^T\boldsymbol{u}}{\lambda}} \\ e^{-j2\pi\frac{\boldsymbol{r}_2^T\boldsymbol{u}}{\lambda}} \\ \vdots \\ e^{-j2\pi\frac{\boldsymbol{r}_M^T\boldsymbol{u}}{\lambda}} \end{bmatrix} \tag{2.11}$$

Results until now can readily be extended for multiple source signals case in a straightforward manner using the superposition principle. Signal model for n sources is given by

$$\boldsymbol{y}(t) = [\boldsymbol{a}(\phi_1,\theta_1)\ \ldots \boldsymbol{a}(\phi_n,\theta_n)] \begin{bmatrix} s_1(t) \\ \vdots \\ s_n(t) \end{bmatrix} + \boldsymbol{n}(t) = \boldsymbol{A}\boldsymbol{s}(t) + \boldsymbol{v}(t) \tag{2.12}$$

where

$$\boldsymbol{A} \triangleq [\boldsymbol{a}(\phi_1,\theta_1)\ \boldsymbol{a}(\phi_2,\theta_2)\ \ldots \boldsymbol{a}(\phi_n,\theta_n)] \tag{2.13}$$

$$\boldsymbol{s}(t) \triangleq [s_1(t)\ s_2(t)\ \ldots\ s_n(t)]^T \tag{2.14}$$

Until now, we assume that signal received from the array is a continuous signal. But usually, sampled version $y_i(t)$ is used by a digital processing equipment for direction of arrival estimation. Block scheme of a simplified hardware structure is given in Fig. 2.3.

We can rewrite the sampled form of the sensor array output as

$$\boldsymbol{y}(k) = \boldsymbol{A}\boldsymbol{s}(k) + \boldsymbol{v}(k) \qquad k = 1, 2 \ldots K \tag{2.15}$$

where K is the number of snapshots obtained from the sensor array.

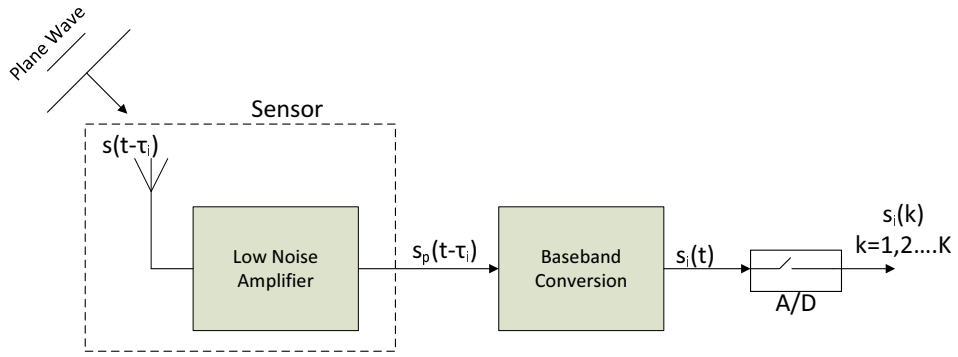

Figure 2.3: A simplified block diagram of a receiver

2.2 A Special Case:Uniform Linear Array

Consider m identical sensors uniformly spaced on the x-axis with the spacing d. Such array is shown in Fig. 2.4 and referred as the **U**niform **L**inear **A**rray(ULA). Let d_i denote the ith sensor position on x-axis which is given by

$$d_i = (i-1)\ d \qquad i = 1, 2, \ldots m \tag{2.16}$$

Assuming that the target is on the same plane($\theta = 90$) with the linear array, array manifold vector for ULA is given by

$$\boldsymbol{a}(\phi) = [1, e^{-j2\pi k cos\phi}, \ldots, e^{-j2\pi(m-1)k cos\phi}] \tag{2.17}$$

where k is the sensor spacing in wavelengths given by

$$k \triangleq \frac{d}{\lambda} \tag{2.18}$$

One important observation about the linear arrays is that same array manifold vector is obtained for any two source symmetrical to the array line hence these sources can not be distinguished from one another.

Let spatial frequency defined as $w_s \triangleq 2\pi k cos(\phi)$. Substituting the w_s into the Eq. 2.17, we get

$$\boldsymbol{a}(\phi) = [1, e^{-jw_s}, \ldots, e^{-j(m-1)w_s}] \tag{2.19}$$

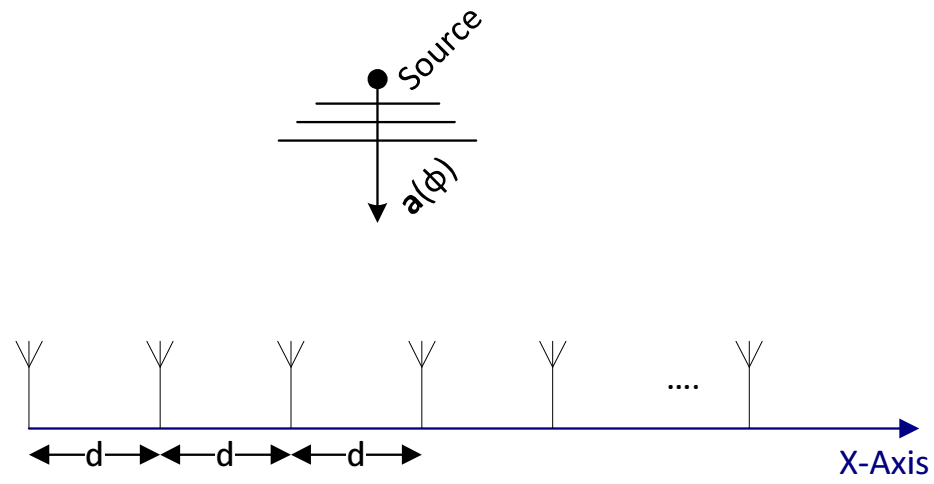

Figure 2.4: Uniform Linear Array of m sensors with sensor spacing d

Note that the manifold vector given in Eq. 2.19 is essentially the samples of a complex sinusoidal signal with frequency w_s. So DOA estimation is simply analogous to the frequency estimation problem. In frequency estimation problem, temporal frequency of the signal is estimated using the samples of the signal whereas in direction finding spatial frequency w_s is estimated using the samples obtained from the sensors.

Analogous to the temporal frequency estimation, Shannon sampling theorem can be extended to the spatial frequency estimation for uniform linear array case. In order to avoid aliasing effects, following condition must be satisfied so that array manifold vector $a(\phi)$ is unique for different direction of arrivals.

$$|w_s| \leq \pi \Longleftrightarrow d \leq \frac{\lambda}{2} \tag{2.20}$$

Condition given in Eq. 2.20 simply states that for ULA, samples in space should be dense enough so that spatial the frequency can be uniquely be determined.

ULA can be thought as the uniform sampling of the wavefield. In this thesis, what we would like to achieve is to find a way to sample the wavefield in a non-uniform matter and still uniquely determine the DOA with no ambiguity. By doing so, we hope to offer a solution to some practical problems. For example, we might be able to get a superior performance compared to the ULA with same number of elements.

CHAPTER 3

AMBIGUITY PROBABILITY AND LINEAR DEPENDENCE OF STEERING VECTORS

In this chapter, we will primarily focus on the ambiguity issue of sensor arrays. In section 3.1, probability of ambiguity is defined and a function relating the array geometry with ambiguity response is given. Obtained results are also supported with simulation results for clarity and validation. In section 3.2, the function related to ambiguity is deeply investigated in order to have a better understanding and provide a basis for the next sections. Further effort has been made in section 3.3, in order to prove that the ambiguity related function is not solely related to ambiguity response but also to the overall array performance.

3.1 Ambiguity Probability

Consider a scenario where one signal impinging on an array of M sensors. Assume that ϕ_1 and ϕ_2 are two different DOA estimate candidates. Using the snapshots $\{\mathbf{y}(k)\}_{k=1}^{K}$, angle of arrival of the signal will be estimated. For both AOA candidates we can write the hypothesis as

$$H_1 : \boldsymbol{y}(k) = \boldsymbol{a}(\phi_1)s(k) + \boldsymbol{v}(k) \qquad k = 1, 2, \ldots, K \tag{3.1}$$

$$H_2 : \boldsymbol{y}(k) = \boldsymbol{a}(\phi_2)s(k) + \boldsymbol{v}(k) \qquad k = 1, 2, \ldots, K \tag{3.2}$$

where we assume that $s(k)$ is a zero mean Gaussian process with $\sigma_s^2 \triangleq E\{s(k)s^*(k)\}$ and noise vector denoted by $\boldsymbol{v}(k)$ is both spatially and temporally white Gaussian process with covariance $E\{\boldsymbol{v}(k)\boldsymbol{v}(k)^H\} = \sigma^2 \boldsymbol{I}_N$.

Covariance matrices of both hypothesis can be written as

$$\boldsymbol{R}_i = \sigma_s^2 \mathbf{a}(\phi_i)\mathbf{a}(\phi_i)^H + \sigma^2 \boldsymbol{I}_N \qquad i = 1, 2 \tag{3.3}$$

In Appendix A, it is proved that minimum probability of making the wrong decision between ϕ_1 and ϕ_2 is achieved by the likelihood test given in Eq. 3.4. Similar derivations are given in [5].

$$\begin{aligned} \epsilon &= tr\{(\boldsymbol{R}_1^{-1} - \boldsymbol{R}_2^{-1})\tilde{\boldsymbol{R}}\} \lessgtr 0 \\ &= \frac{1}{K}\sum_{k=1}^{K} \boldsymbol{y}^H(\boldsymbol{R}_1^{-1} - \boldsymbol{R}_2^{-1})\boldsymbol{y} \lessgtr 0 \end{aligned} \tag{3.4}$$

where $\tilde{\boldsymbol{R}} \triangleq \frac{1}{K}\sum_{k=1}^{K} \boldsymbol{y}\boldsymbol{y}^H$ denotes the sample covariance matrix.

ϵ given in Eq. 3.4 is just a sum of K random variables and according to central limit theorem its distribution converges to normal distribution for large enough snapshots. For both hypothesis, decision regions and distribution of ϵ are shown in Fig. 3.1.

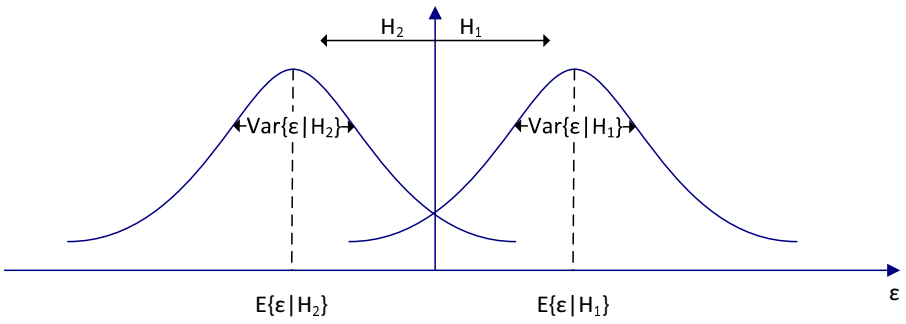

Figure 3.1: Decision Regions and Distributions for Two Hypothesis

Assuming that ϕ_2 is the true AOA, probability of choosing the wrong AOA angle ϕ_1 is given by(see Appendix A for proof),

$$\begin{aligned} P_a &= Prob\{\epsilon > 0 | H_2\} \\ &= \Phi\left(\sqrt{\frac{K}{1 + \frac{2}{p(1-\beta^2)}}}\right) \end{aligned} \tag{3.5}$$

where

$$\beta(\phi_1, \phi_2) \triangleq \frac{|\boldsymbol{a}(\phi_1)^H \boldsymbol{a}(\phi_2)|}{M} \tag{3.6}$$

$$p \triangleq \frac{(\frac{M\sigma_s^2}{\sigma^2})^2}{1 + \frac{M\sigma_s^2}{\sigma^2}} = \frac{(M \cdot SNR)^2}{1 + M \cdot SNR} \tag{3.7}$$

$$\Phi(x) \triangleq \frac{1}{2\pi} \int_x^\infty \exp^{-\frac{t^2}{2}} dt \tag{3.8}$$

$\Phi(x)$ given in Eq. 3.8 is known as complementary error function.

Considering the Eq. 3.5 following comments can be made on the probability of ambiguity.

- Probability of ambiguity is a increasing function of β and it is the only variable related to array geometry.
- Ambiguity probability decreases as SNR and number of snapshots increases.
- It is not meaningful to give the error probability of a sensor array without mentioning the other parameters. Signal power, noise power and number of snapshots must be given in order to determine the error probability.
- Note that, derivations until now does not include any assumption about the relation between ϕ_1 and ϕ_2. As a definition, ambiguities are only defined between widely separated angles. But probability values are also valid for closely separated angles and it directly affects the estimation accuracy of the array. This property will be further investigated in the upcoming sections.
- Every sensor array will start producing significant number of large DOA errors after some threshold for low SNR and/or insufficient number of snapshots. Depending on the β value, threshold values of SNR and number of snapshots will change.

In order to validate the results, Monte Carlo experiments are done for hypothesis testing using a minimum redundant linear array positioned on x-axis with element positions $\boldsymbol{d} = [0, \frac{\lambda}{2}, 2\lambda, 3\lambda]$. During the simulations true direction of arrival value, Φ_2, is used to generate noisy snapshots while the false DOA ϕ_1 is kept constant. For different

angle combinations $\{\phi_1, \phi_2\}$, value of the function $\beta(\phi_1, \phi_2)$ changes depending on the array geometry. Simulation parameters are given in Table 3.1. Corresponding values $\beta(\phi_1, \phi_2)$ are calculated using Eq. 3.6 for the parameters given in Table 3.1.

Table3.1: Monte Carlo Simulation Parameters for Ambiguity Probability

Parameters	Description	Value
ϕ_1(deg)	False DOA in Hypothesis Testing	90
ϕ_2(deg)	True DOA used for Measurement Generation	[91,120]
SNR(dB)	-	-10 and -20
# of Snapshots	-	100
# of Experiments	Experiments for every ϕ_1, ϕ_2 combinations	$1e4$

In Fig. 3.2, probability of choosing the wrong direction of arrival is plotted. Both Monte Carlo simulation results and the values calculated using complementary error function is given. Results confirms that error probability function given in Eq. 3.5 is valid.

In Fig. 3.3, probability of choosing wrong direction of arrival and $\beta(90, \phi_2)$ is plotted for all ϕ_2 values. It can be seen that, regardless of the true direction of arrival, ϕ_2, same probability of wrong decision obtained when β value is constant.

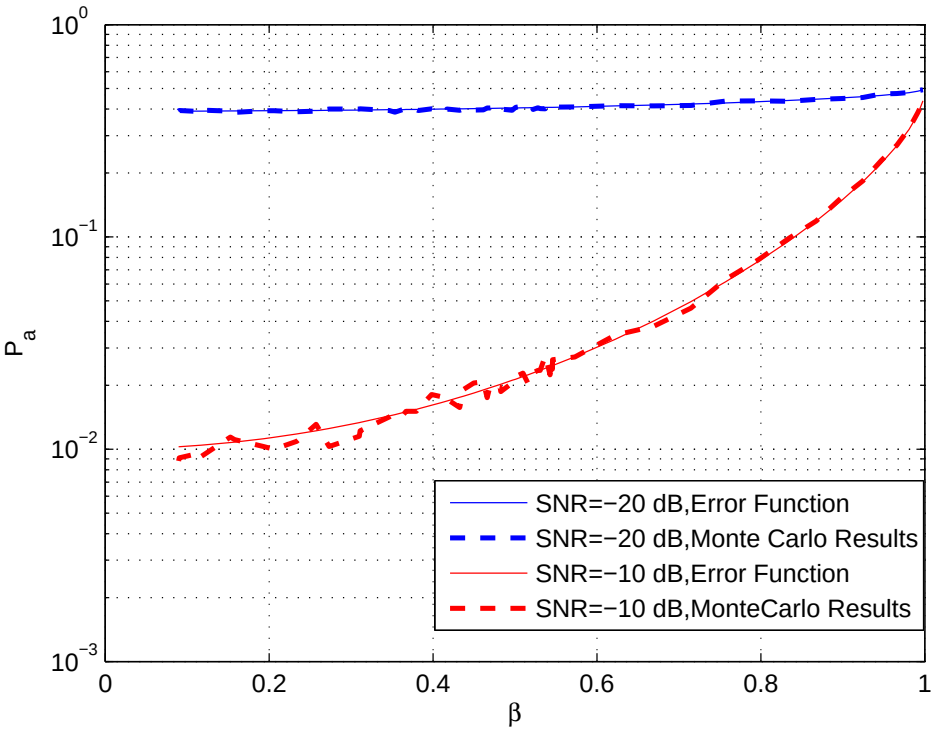

Figure 3.2: Probability of Ambiguity for Minimum Redundant Linear Array

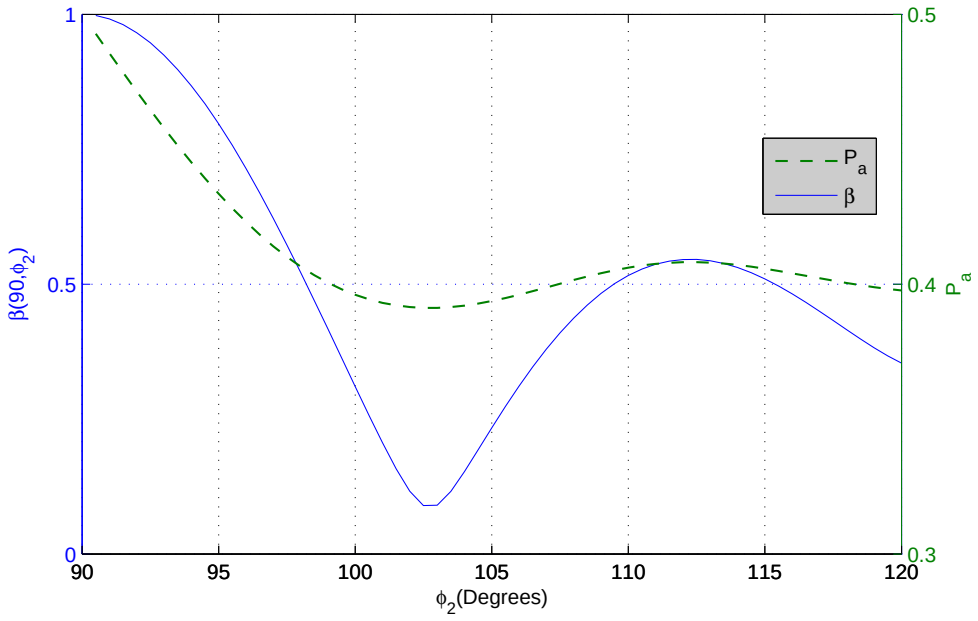

Figure 3.3: β Values and P_a Corresponding to ϕ_2, SNR=-20 dB

3.2 Significance of Beta Function and Linear Dependence of Steering Vectors

In previous section, it is proved that probability of choosing the wrong angle of arrival is directly related to a function $\beta(\phi_1, \phi_2)$ given in Eq. 3.6. In this section, this function will be further investigated in order to understand its relation with ambiguity, estimation accuracy and resolution of the sensor array.

Let $J(\phi_1, \phi_2)$ be defined as

$$J(\phi_1, \phi_2) \triangleq \boldsymbol{a}(\phi_1)^H \boldsymbol{a}(\phi_2) \tag{3.9}$$

Note that $J(\phi_1, \phi_2)$ is essentially the inner product of two vectors, formally $J(\phi_1, \phi_2) : \mathbb{C}^M \times \mathbb{C}^M \rightarrow \mathbb{R}$.

The Cauchy-Schwarz inequality states that for all vectors x and y of an inner product space it is true that

$$|\langle x, y\rangle| \leq \langle x, x\rangle \langle y, y\rangle \tag{3.10}$$

So following inequality holds for $J(\phi_1, \phi_2)$.

$$|\mathbf{a}(\phi_1)^H \mathbf{a}(\phi_2)| \leq \|\mathbf{a}(\phi_1)\| \|\mathbf{a}(\phi_2)\| \tag{3.11}$$

Moreover, strict equality holds when $\mathbf{a}(\phi_1)$ and $\mathbf{a}(\phi_2)$ are linearly dependent or formally $\mathbf{a}(\phi_1) = \alpha \mathbf{a}(\phi_2)$ where $\alpha \in \mathbb{C}$.

Steering vector of a M element linear sensor array is given by

$$\mathbf{a}(\phi) = [e^{j2\pi k_1 cos(\phi)}, e^{j2\pi k_2 cos(\phi)}, \cdots, e^{j2\pi k_M cos(\phi)}] \tag{3.12}$$

where k_i represents ith sensor position in wavelengths. Norm of the steering vector can be calculated as

$$\|\mathbf{a}(\phi)\| = \sqrt{\sum_{i=1}^{M} |e^{j2\pi k_i cos(\phi)}|^2} = \sqrt{M} \tag{3.13}$$

Substituting Eq. 3.13 into Eq. 3.11 we get,

$$|\mathbf{a}(\phi_1)^H \mathbf{a}(\phi_2)| \leq M \tag{3.14}$$

Using the result in Eq. 3.14 and property of absolute value operator, we can write the following inequality for $\beta(\phi_1, \phi_2)$.

$$0 \leq \beta(\phi_1, \phi_2) \leq 1 \tag{3.15}$$

Depending on the values of β, we can make the following comments on the linear dependence of steering vectors.

- β value increases as linear dependence of steering vectors increases. When $\beta = 1$, steering vectors become linearly dependent.
- β becomes 0 when steering vectors are orthogonal.

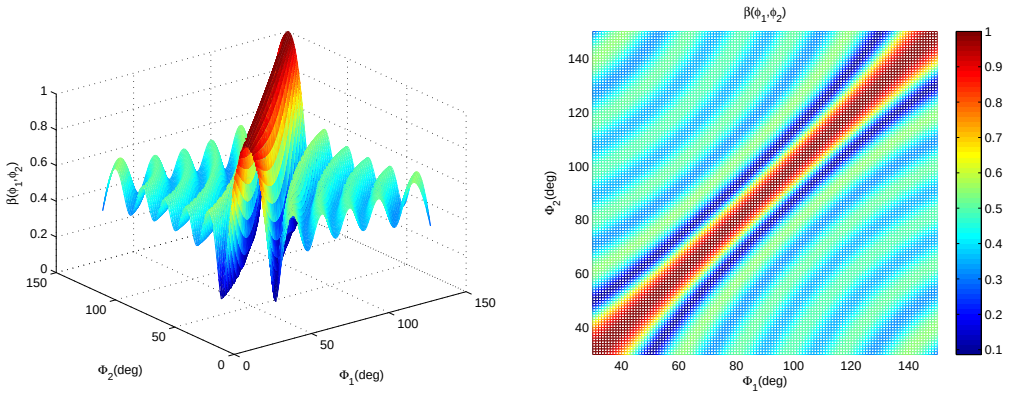

(a) $\beta(\phi_1, \phi_2) for Minimum Redundant Array$ (b) $\beta(\phi_1, \phi_2)$, Top View

Figure 3.4: $\beta(\phi_1, \phi_2)$ for Minimum Redundant Array with Element Positions $\boldsymbol{d} = [0, \frac{\lambda}{2}, 2\lambda, 3\lambda]$ and $\phi_1, \phi_2 \in [30, 150]$

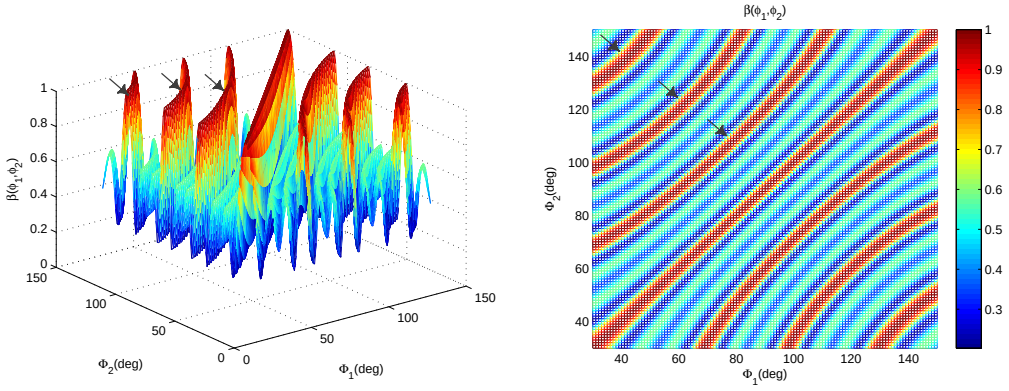

(a) $\beta(\phi_1, \phi_2) for Ambiguous Redundant Array$ (b) $\beta(\phi_1, \phi_2)$, Top View

Figure 3.5: $\beta(\phi_1, \phi_2)$ for Linear Ambiguous Array with Element Positions $\boldsymbol{d} = [0, 2\lambda, 6\lambda]$ and $\phi_1, \phi_2 \in [30, 150]$

In Fig. 3.4, $\beta(\phi_1, \phi_2)$ is illustrated for a 4 element minimum redundant array. Diagonal terms in the plot are the $\{\phi_1, \phi_2\}$ pairs that are close and as expected they are linearly dependent. As $|\phi_1 - \phi_2|$ increases, $\beta(\phi_1, \phi_2)$ becomes smaller and steering vectors become linearly independent. One can also observe that there is no largely separated angles with large $\beta(\phi_1, \phi_2)$. So this array will have satisfactory ambiguity response. However, this observation is not true for Fig. 3.5. There are linearly dependent steering vectors with widely separated angles and this array will produce large DOA errors with high probability even at high SNR with large number of snapshots.

3.2.1 Relation Between Beta Function and Data Independent Beamformer

People working in array processing area might feel quite familiar when they first see the Eq. 3.6 because $\beta(\phi_1, \phi_2)$ might be thought as a magnitude response of a conventional data independent beamformer for steering angle ϕ_1 and emitter DOA ϕ_2.

In order to show the relation between $\beta(\phi_1, \phi_2)$ and DOA accuracy, we first introduce deterministic maximum likelihood(ML) DOA estimator. For single source case, data independent beamformer is the ML estimator for direction of arrival. Although this is a well know result, proof is given in Appendix B for completeness.

$$\begin{aligned} \hat{\phi} &= \underset{\phi_D}{\operatorname{argmax}} \left\{ \frac{1}{K} \sum_{k=1}^{K} |\boldsymbol{y}_f(k)|^2 \right\} \\ &= \underset{\phi_D}{\operatorname{argmax}} \left\{ \frac{1}{K} \sum_{k=1}^{K} |\frac{\boldsymbol{a}(\phi_D)^H}{\sqrt{M}} \boldsymbol{y}(k)|^2 \right\} \end{aligned} \tag{3.16}$$

where $\boldsymbol{y}_F \triangleq \frac{1}{\sqrt{M}} \boldsymbol{a}(\phi_D)^H \boldsymbol{y(t)}$ denotes the signal at the output of the beamformer for direction ϕ_D and direction in which the output power of the beamformer is maximized will be selected as the estimated AOA. For ML estimation, as it can be seen in Eq. 3.16, beamformer weights are chosen to be the normalized steering vectors of the related direction which is also known as the data independent beamformer.

Beam pattern of a such beamformer when array is steered to direction ϕ_D is given by

$$\begin{aligned} B(\phi) &= |\boldsymbol{w}^H \boldsymbol{a}(\phi)|^2 \\ &= \frac{|\boldsymbol{a}(\phi_D)^H \boldsymbol{a}(\phi)|^2}{M} \end{aligned} \tag{3.17}$$

Now comparing the Eq. 3.6 and Eq. 3.17, we see that they are essentially the same thing. By identifying this similarity, we can look at the ambiguity problem from

another point of view. Ambiguity problem can be seen as determining the geometry of a sensor array such that when array steered to each direction in its operation range, side lobes of the beam pattern should be suppressed enough so that leakage from other angles is prevented. In Fig. 3.4 and Fig. 3.5, $\beta(\phi_1, \phi_2)$ function is given for two different arrays. Each cuts of these graphs are actually the beam pattern for different steering angles. In Fig. 3.6, beam pattern for boresight steering is given. For the ambiguous array we see that side lobes are as high as the main lobe, so when steered to some angle, emitter signal coming from some other direction will just leak in and DOA estimator given in Eq. 3.16 will not be able to distinguish the true angle of arrival.

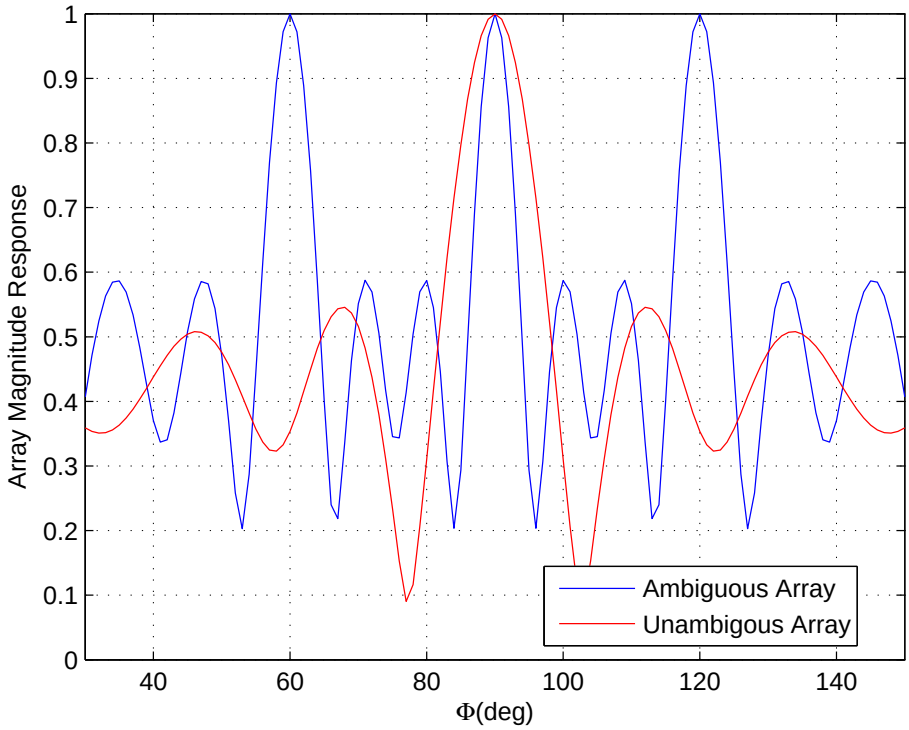

Figure 3.6: Comparison of Beam Patterns between Ambiguous and Unambiguous Linear Arrays

Noticing the similarity between data independent beamformer and $\beta(\phi_1, \phi_2)$ does not only give us another point of view but also gives us an opportunity to relate $\beta(\phi_1, \phi_2)$ with DOA estimation accuracy and resolution limit of the sensor array. In section 3.3, relation between beam pattern and array performance is studied in detail.

3.3 Array Resolution and Estimation Accuracy

Until now, we mainly focused on large direction of arrival errors and proved that they can be characterized using the function $\beta(\phi_1, \phi_2)$. But during the derivations of ambiguity probability, no assumption about the relationship between ϕ_1 and ϕ_2 is made. So these probabilities are also valid for closely separated angles. Intuitively, one can think that $\beta(\phi_1, \phi_2)$ for closely separated angles should determine the DOA estimation accuracy and the resolution of array. In this section, it will be proved that this idea is correct and just by looking the figures given in 3.4 and 3.5, one can comment on both the resolution and accuracy of the related sensor array.

First we need to clearly express the distinction between resolution and accuracy. Estimation accuracy is not sufficient to characterise the performance of a DF system when multiple signals are present and in such cases, resolution of the array should also be considered. In [1, 7], resolution is defined as the ability of a system to distinguish between tightly spaced emitters. In [1, 8, 9], it is stated that resolution is closely related to determination of the number of distinct components in the composite signal received by the array whereas accuracy is related to detection or decision. In order to estimate the DOA of emitters, it is first necessary to determine the number of different DOAs included in the composite signal which is related to resolution. Algorithms like MUSIC[10] or MLE[11] assume that number of sources is known and accepts this information as an input.

Usually, accuracy of a direction finding system is expressed in terms of mean-square error(MSE) which is given by

$$MSE\{\hat{\phi}\} \triangleq E\{|\hat{\phi} - \phi|^2\} \tag{3.18}$$

where $\hat{\phi}$ denotes the estimated DOA and ϕ denotes the true DOA.

Cramer-Rao bound(CRB)[12] is also an important tool for assessing the accuracy of parameter estimation methods, as it provides a lower bound on the accuracy of any unbiased estimator.

$$MSE\{\hat{\phi}\} = VAR\{\hat{\phi}\} \geq CRB \tag{3.19}$$

In [1], CRB for direction finding problem is given as

$$CRB(\phi) \approx \frac{1}{2KSNR\,|\dot{\boldsymbol{a}}(\phi)|^2} \tag{3.20}$$

where K is the number of snapshots and $\dot{\boldsymbol{a}}(\phi)$ denotes the derivative of the array manifold with respect to DOA angle ϕ. We see that CRB is inversely proportional to the factor $\dot{\boldsymbol{a}}(\phi)$. This relation tells us that if the steering vectors are changing fast, DF system will have the ability to estimate the DOA more accurately.

Beamwidth of the array is another parameter of the array which depends on the rate of change of steering vectors. So we can relate the CRB with beamwidth of the array as well. In [13], relation between CRB and 3dB beamwidth of the array is given by.

$$CRB \propto BW^2 \tag{3.21}$$

where BW denotes the beamwidth of the sensor array. Similar relations between beamwidth and CRB is also given [14, 15].

Resolution limit Δ_{r} is usually defined as the minimum angular separation between two sources required in order to satisfy a correct detection probability. As for the CRB case, numerous efforts[16, 17, 18, 19] have been made to define the resolution limit, Δ_{r} in terms of known array parameters. In [20, 21], authors stated that resolution limit is proportional to

$$\Delta_{\mathrm{r}} \propto \frac{BW}{SNR^{\frac{1}{4}}} \tag{3.22}$$

In Eq. 3.22, relation is given for the single snapshot case. But it is always possible to calculate the overall SNR for K snapshots and the equation will be still valid.

In literature, there are studies about the relationship between beamwidth and resolution limit. For example, in [16] authors showed that resolution limit is inversely proportional to square root of SNR rather than the fourth root. These relations are heavily dependent on how resolution limit is defined and signal parameters used during the derivations. But in [1], it is stated that the resolution limit given in Eq. 3.22 is achievable in most practical problems.

In order to have better understanding of the relation between beamwidth, resolution and accuracy, some simulations are made. During the simulations 4 element and 8 element uniform linear arrays(ULA) with spacing $\lambda/2$ are compared in terms of

beamwidth, accuracy and resolution. In Fig. 3.7, direction finding accuracy of both arrays are given. During the simulations, MUSIC[10] is used as the DOA estimator. Note that accuracy of estimation is given in root mean square(RMS) sense in Fig. 3.7. Using the relation given in Eq. 3.19, relation between root mean square error(RMSE) can be found as

$$RMSE \propto BW \tag{3.23}$$

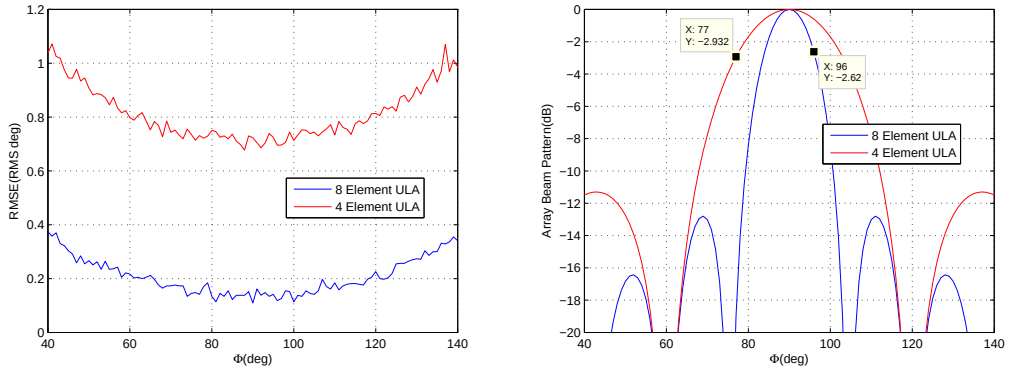

(a) DF Accuracy for 4 Element and 8 Element ULA, 0 dB SNR, 100 Snapshots

(b) Beam Patterns of 4 Element and 8 Element ULA for 90 degree(boresight) steering angles

Figure 3.7: DF Accuracy and Beam Width Comparison of Two Different ULAs

Simulation result given in Fig. 3.7 is obtained when elements of the array positioned on the x-axis. So when $\phi = 90$ degree, narrowest beamwidth is obtained for both arrays. As a result, best DOA accuracy is obtained for boresight angle.

Detailed analysis and simulations for resolution limit will not be given here as definition of resolution limit depends on different parameters and assumptions which is outside the scope of this thesis. Instead, in order to show that smaller beamwidth provides better resolution, we compared the MUSIC spectrum of a scenario with two closely separated emitters in Fig. 3.8. It can be seen that, 8 element array able to resolve two emitters whereas 4 element fails to produce two separate peaks in its spectrum.

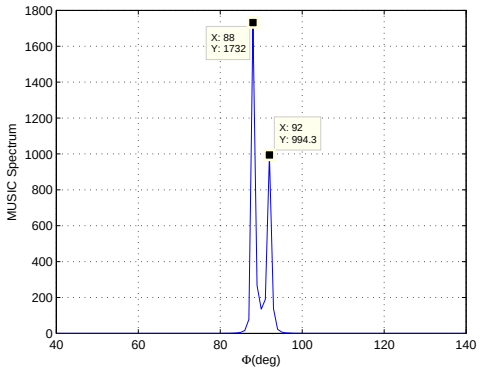

(a) MUSIC Spectrum of 8 Element Array

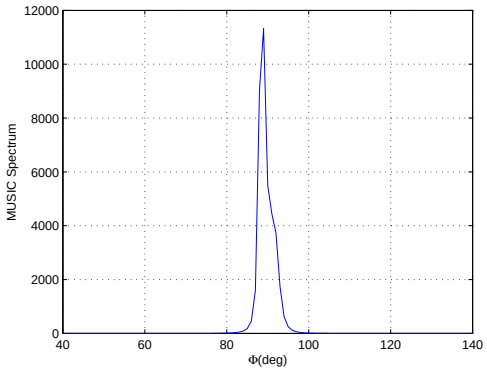

(b) MUSIC Spectrum of 4 Element Array

Figure 3.8: MUSIC Spectrum for 8 Element and 4 Element ULA, SNR = 20 dB, K=100 Snapshots, Emitter Angles=[88,92] degrees

3.4 Approximation of Beta Function

In previous sections, $\beta(\phi_1, \phi_2)$ given in Eq. 3.6 is shown to be directly related to ambiguity probability and array performance. Now we are going to give an approximation for this function which is valid for large values of $\beta(\phi_1, \phi_2)$.

In Eq. 3.9, function $J(\phi_1, \phi_2)$ defined as $J(\phi_1, \phi_2) \triangleq \boldsymbol{a}(\phi_1)^H \boldsymbol{a}(\phi_2)$. Substituting Eq. 3.9 into Eq. 3.6 we get,

$$\beta(\phi_1, \phi_2) = \frac{|J(\phi_1, \phi_2)|}{M} \tag{3.24}$$

Substituting Eq. 3.12 into $|J(\phi_1, \phi_2)|$, we get

$$\begin{aligned} |J(\phi_1, \phi_2)| &= \left|\boldsymbol{a}(\phi_1)^H \boldsymbol{a}(\phi_2)\right| \\ &= \left|\sum_{i=1}^{M} e^{j2\pi k_i \gamma}\right| \\ &= \left[\left(\sum_{i=1}^{M} cos(2\pi k_i \gamma)\right)^2 + \left(\sum_{i=1}^{M} sin(2\pi k_i \gamma)\right)^2\right]^{\frac{1}{2}} \end{aligned} \tag{3.25}$$

where γ is defined as $\gamma \triangleq cos(\phi_2) - cos(\phi_1)$ and we use the fact that $|J(\phi_1, \phi_2)|^2 = \Re\{J(\phi_1, \phi_2)\}^2 + \Im\{J(\phi_1, \phi_2)\}^2$.

Now let us redefine steering vectors by placing the first element on the origin of the coordinate system.

$$\mathbf{a}(\phi) = [1, e^{j2\pi k_2 cos(\phi)}, \cdots, e^{j2\pi k_M cos(\phi)}] \tag{3.26}$$

where k_i is the sensor position of ith sensor with respect to the first element normalized with the wavelength.

By writing the steering vectors as in Eq. 3.26, we actually restrain the phase rotation of each element. In order words, we use the first element as a reference and phase difference of each element must now be constant with respect to the first element of the array. And also phase of the first element must be 0 for all angles as $k_0 = 0$.

Considering the Eq. 3.25 and Eq. 3.26 together, one can see that $|J(\phi_1, \phi_2)|$ will be large and ambiguity probability will be significant whenever the phases of steering vectors $\mathbf{a}(\phi_1)$ and $\mathbf{a}(\phi_2)$ are the same, formally when $mod(2\pi k_i \gamma)_{(2\pi)} \ll 1,\ i = 1, 2, \ldots M$. In other words, writing the steering vectors with respect to first element, steering vectors become linearly dependent whenever they are the same.

Under the conditions above, $\Re\{J(\phi_1, \phi_2)\}$ will be dominant in Eq. 3.25 and approximation of $J(\phi_1, \phi_2)$ is given by

$$\begin{aligned} \tilde{J}(\phi_1, \phi_2) &\triangleq \sum_{i=1}^{M} cos(2\pi k_i \gamma) \\ &= \Re\{\mathbf{a}(\phi_1)^H \mathbf{a}(\phi_2)\} \end{aligned} \tag{3.27}$$

Substituting Eq. 3.27 into Eq. 3.6, we get the approximation for the β function as

$$\tilde{\beta}(\phi_1, \phi_2) \triangleq \frac{\sum_{i=1}^{M} cos(2\pi k_i \gamma)}{M} = \frac{\Re\{\mathbf{a}(\phi_1)^H \mathbf{a}(\phi_2)\}}{M} \tag{3.28}$$

This approximation is quite useful for our purposes because we are mostly interested with the region in which $\beta(\phi_1, \phi_2)$ takes large values due to the fact that both ambiguity probability and array performance is defined by this region as shown in previous sections. In Fig. 3.9, both $\beta(\phi_1, \phi_2)$ and $\tilde{\beta}(\phi_1, \phi_2)$ are given for an ambiguous array. It can be seen that, for large values of β, both functions are almost the same.

Approximation in Eq. 3.28 is also used in [5, 6] in order to relate the Euclidean distance with ambiguity related function $\beta(\phi_1, \phi_2)$. When we write steering vectors as in Eq. 3.26, Euclidean distance between and two steering vector is also directly related to the

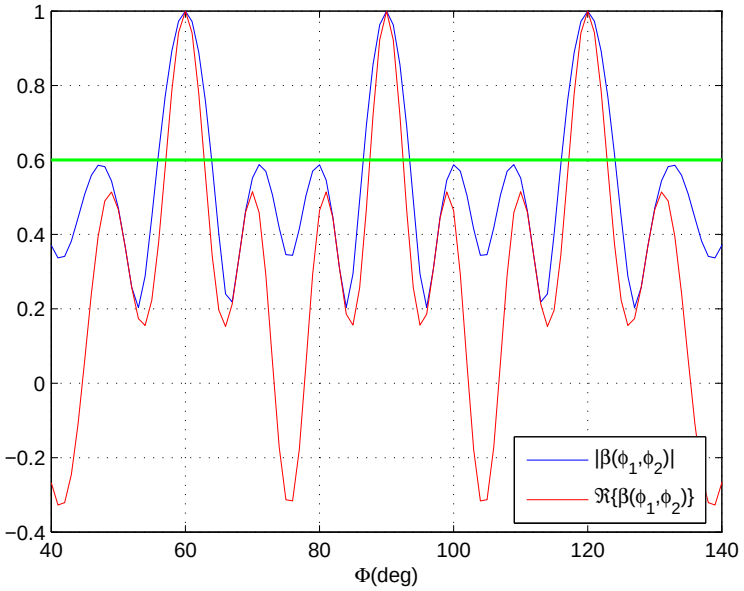

Figure 3.9: Real and absolute value of $\beta(90, \phi_2)$ for sensor array with element positions $\boldsymbol{d} = [0, 2\lambda, 6\lambda]$

probability ambiguity. Euclidean distance between two steering vectors is given by

$$\begin{aligned} \|\mathbf{a}(\phi_1) - \mathbf{a}(\phi_2)\|^2 =& [\mathbf{a}(\phi_1) - \mathbf{a}(\phi_2)]^H [\mathbf{a}(\phi_1) - \mathbf{a}(\phi_2)] \\ =& \mathbf{a}^H(\phi_1)\mathbf{a}(\phi_1) + \mathbf{a}^H(\phi_2)\mathbf{a}(\phi_2) \\ & -(\mathbf{a}^H(\phi_1)\mathbf{a}(\phi_2) + \mathbf{a}^H(\phi_2)\mathbf{a}(\phi_1)) \end{aligned} \tag{3.29}$$

where

$$\mathbf{a}^H(\phi_1)\mathbf{a}(\phi_1) = \mathbf{a}^H(\phi_2)\mathbf{a}(\phi_2) = M \tag{3.30}$$

$$\mathbf{a}^H(\phi_1)\mathbf{a}(\phi_2) = (\mathbf{a}^H(\phi_2)\mathbf{a}(\phi_1))^* \tag{3.31}$$

$$\mathbf{a}^H(\phi_1)\mathbf{a}(\phi_2) + \mathbf{a}^H(\phi_2)\mathbf{a}(\phi_1) = 2\Re\{\mathbf{a}^H(\phi_1)\mathbf{a}(\phi_2)\} \tag{3.32}$$

Substituting Eq. 3.30,3.32 into 3.29 we get,

$$\|\mathbf{a}(\phi_1) - \mathbf{a}(\phi_2)\|^2 = 2\ (M - \Re\{\mathbf{a}^H(\phi_1)\mathbf{a}(\phi_2)\}) \tag{3.33}$$

Comparing Eq. 3.28 and Eq. 3.33, one can observe that they have quite similar characteristics except Euclidean distance is small when steering vectors are linearly dependent whereas $\beta(\phi_1, \phi_2)$ is large. In Fig. 3.10, comparison between Euclidean distance and $\Re\{\beta(\phi_1, \phi_2)\}$ is given.

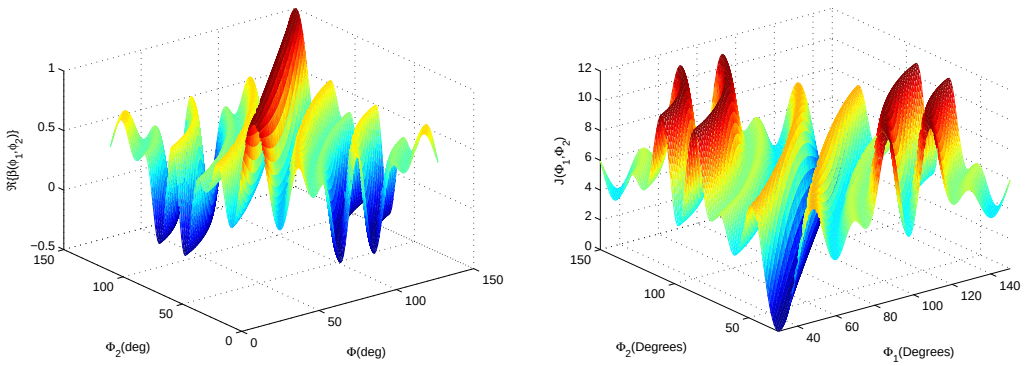

(a) Real Part of $\beta(\phi_1, \phi_2)$

(b) Euclidean Distance of Steering Vectors

Figure 3.10: Comparison between Euclidean Distance and $\Re\{\beta(\phi_1, \phi_2)\}$ for the sensor array with element positions $\boldsymbol{d} = [0, 2\lambda, 6\lambda]$

CHAPTER 4

SPARSE ARRAY DESIGN USING BINARY PROGRAMMING

4.1 Linear Unambiguous Array Design

Consider the scenario given in Fig.4.1 where linear array of m sensors are placed on the x-axis with spacing Δ_L and maximum aperture L.

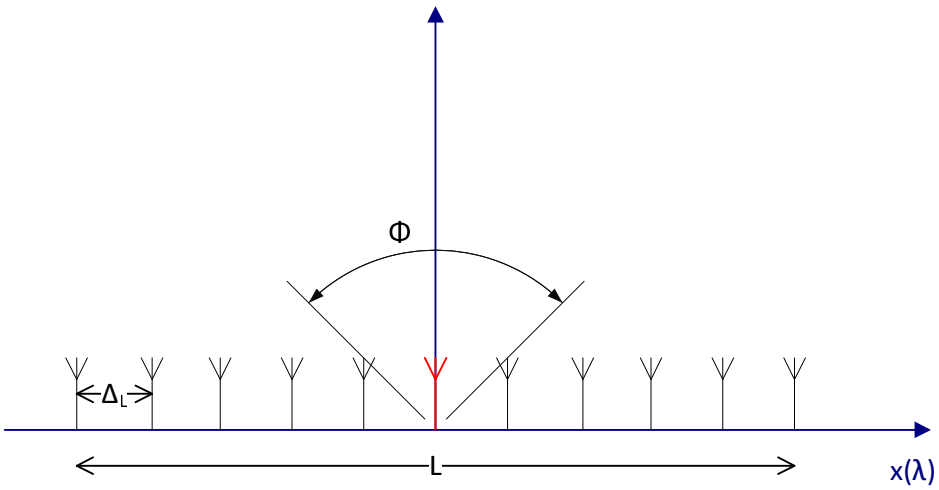

Figure 4.1: Linear Sensor Grid of m elements with aperture size L

Assume that, using the elements of this array, azimuth angle of arrival will be estimated. Let Φ denote the interval of azimuth angles that the array is going to operate.

$$\Phi \triangleq [\phi_{min}, \phi_{max}] \tag{4.1}$$

Assuming that the first element is positioned at the origin of the coordinate system,

array manifold is given by

$$\mathbf{a}(\phi) = [1, e^{j2\pi k_2 cos(\phi)}, e^{j2\pi k_3 cos(\phi)}, \cdots, e^{j2\pi k_m cos(\phi)}] \tag{4.2}$$

where k_i is the sensor position of ith sensor on x-axis normalized with the wavelength.

Note that in Eq. 4.2, term corresponding the first element is always the same and last (m-1) term characterizes the manifold vector as given below.

$$\mathbf{g}(\phi) \triangleq [e^{j2\pi k_2 cos(\phi)}, e^{j2\pi k_3 cos(\phi)}, \cdots, e^{j2\pi k_m cos(\phi)}] \tag{4.3}$$

What we would like to achieve is to determine which sensor spacings k_i to use in order to have unambiguous array response. In order to do that, we introduce sensor gains that are either 0(off) or 1(on) in Eq. 4.3, i.e,

$$\mathbf{g}(\phi) = [x_2 e^{j2\pi k_2 cos(\phi)}, x_3 e^{j2\pi k_3 cos(\phi)}, \cdots, x_m e^{j2\pi k_m cos(\phi)}] \tag{4.4}$$

where x_i denotes the ith sensor gain. Let the sensor gain vector be defined as

$$\boldsymbol{x} \triangleq [x_2 \ x_3 \ \cdots \ x_m]^T \tag{4.5}$$

Note that first element phase and gain are not included in both Eq. 4.4 and Eq. 4.5. In order to make our previous assumptions still valid, we assume that $x_1 = 1$ and sensor on the origin does always exist.

By adding the sensor gains into Eq. 3.26, we transform the unambiguous array problem from determining the sensor spacings k_i into determining the sensor gain vector $\boldsymbol{x}$.

We define the sparse unambiguous array design problem as

(P_1)

$$\begin{aligned} \underset{\mathbf{x}}{\text{minimize}} \quad & \|\mathbf{x}\|_0 \\ \text{subject to} \quad & \beta(\phi_1, \phi_2) \leq \bar{\beta}, \ \{\phi_1, \phi_2\} \in \Upsilon \\ & x_i \in \{0, 1\} \end{aligned} \tag{4.6}$$

where Υ is the set $\{\phi_1, \phi_2\}$ couples that are widely separated, formally

$$\Upsilon \triangleq \{(\phi_1, \phi_2) \mid \phi_1 \in \Phi, \phi_2 \in \Phi, |\phi_1 - \phi_2| \geq \sigma\} \tag{4.7}$$

and $\beta(\phi_1, \phi_2)$ is the ambiguity related function approximately given by

$$\beta(\phi_1, \phi_2) \approx \frac{\tilde{J}(\phi_1, \phi_2)}{M} \tag{4.8}$$

where

$$M = \sqrt{\mathbf{a}^H(\phi_1)\mathbf{a}(\phi_1)\mathbf{a}^H(\phi_2)\mathbf{a}(\phi_2)} \tag{4.9}$$

$$\tilde{J}(\phi_1, \phi_2) \triangleq \Re\{\mathbf{a}(\phi_1)^H\mathbf{a}(\phi_2)\} \tag{4.10}$$

Note that M and m are distinct variables and m shows the number of sensor in the starting sensor grid array while M represents the number of sensors used in the designed array.

Optimization problem (P_1) given in Eq. 4.6 can be simplified by making some observations and some algebraic manipulations.

We start by first looking into the objective function of (P_1). As a objective function, ℓ_0 norm is used because it counts the number of non-zero elements in a vector and it is a measure of sparsity. But notice that every element in sensor gain vector $\boldsymbol{x}$ is either 0 or 1. For such a vector ℓ_0 norm is equivalent to ℓ_1 norm. Using this result, equivalent problem (P_2) can be written as

(P_2)

$$\begin{aligned} \underset{\mathbf{x}}{\text{minimize}} \quad & \|\mathbf{x}\|_1 \\ \text{subject to} \quad & \tilde{\beta}(\phi_1, \phi_2) \leq \bar{\beta},\ \{\phi_1, \phi_2\} \in \Upsilon \\ & x_i \in \{0, 1\} \end{aligned} \tag{4.11}$$

Now we start looking into the constraint function $\tilde{\beta}(\phi_1, \phi_2) \leq \bar{\beta}$. Substituting steering

vectors with sensor gains into Eq. 4.9 and Eq. 4.10 assuming $x_1 = 1$, we get

$$\begin{aligned}
\tilde{J}(\phi_1, \phi_2) &= \Re\{\mathbf{a}^H(\phi_1)\mathbf{a}(\phi_2)\} \\
&= \sum_{i=1}^{m} \Re\{x_i^2 e^{2\pi k_i(\cos\phi_2 - \cos\phi_1)}\} \\
&= 1 + \sum_{i=2}^{m} x_i^2 \cos\left(2\pi k_i(\cos\phi_2 - \cos\phi_1)\right) \\
&= 1 + \Re\{\mathbf{g}^H(\phi_1)\mathbf{g}(\phi_2\}
\end{aligned} \tag{4.12}$$

$$\begin{aligned}
M &= \sum_{i=1}^{m} x_i^2 \\
&= 1 + \sum_{i=2}^{m} x_i^2
\end{aligned} \tag{4.13}$$

So ambiguity related function given in Eq. 4.8 becomes

$$\tilde{\beta}(\phi_1, \phi_2) = \frac{1 + \sum_{i=2}^{m} x_i^2 \cos\left(2\pi k_i(\cos\phi_2 - \cos\phi_1)\right)}{1 + \sum_{i=2}^{m} x_i^2} \tag{4.14}$$

Let the sensor power vector be defined as

$$\boldsymbol{p} \triangleq [x_2^2 \; x_3^2 \; \cdots \; x_m^2]^T \tag{4.15}$$

Note that sensor gain vector given in Eq. 4.5 and sensor power vector given in Eq. 4.15 are essentially the same when sensor gains x_i have binary values due to the fact that $x_i^2 = x_i$. So x_i^2 values in Eq. 4.14 can be interchanged with x_i.

$$\tilde{\beta}(\phi_1, \phi_2) = \frac{1 + \sum_{i=2}^{m} x_i \cos\left(2\pi k_i(\cos\phi_2 - \cos\phi_1)\right)}{1 + \sum_{i=2}^{m} x_i} \leq \bar{\beta} \tag{4.16}$$

When we look into the Eq. 4.16, we see that it is a fraction of two linear functions of optimization parameters x_i's. In this form, optimization problem (P_2) given in Eq. 4.11 is not solvable. In order to put it in a solvable form, instead of adding the ambiguity constraints as a fraction of two linear functions, we add numerator and

denominator of Eq. 4.16 as two independent linear constraints as given below.

$$T(\phi_1, \phi_2) \triangleq \Re\{\boldsymbol{g}(\phi_1)^H \boldsymbol{g}(\phi_2)\} = \sum_{i=2}^{m} x_i \cos\left(2\pi k_i(\cos\phi_2 - \cos\phi_1)\right) \leq \bar{T} \tag{4.17}$$

$$Q \triangleq \sum_{i=2}^{m} x_i \geq \bar{Q} \tag{4.18}$$

where

$$\bar{\beta} \triangleq \frac{\bar{T}+1}{\bar{Q}+1} \tag{4.19}$$

If the constraints given in Eq. 4.17 and Eq. 4.18 are both satisfied, constraint in Eq. 4.16 will eventually be satisfied. But note that, Q function given Eq. 4.18 is the same as the objective function of the optimization problem (P_2). By introducing the ambiguity constraint as two independent linear constraints, we limit the minimum number of sensors to be used. Depending on the structure of the problem, new problem (P_3) might only be able to find a sub optimal solution of the problem (P_2). Yet we can still find very sparse arrays by choosing the minimum number of sensors small.

So we can redefine the optimization problem as

(P_3)

$$\begin{aligned} \underset{\mathbf{x}}{\text{minimize}} \quad & \|\mathbf{x}\|_1 \\ \text{subject to} \quad & T(\phi_1, \phi_2) \leq \bar{T},\ \{\phi_1, \phi_2\} \in \Upsilon \\ & \sum_{i=2}^{m} x_i \geq \bar{Q} \\ & x_i \in \{0, 1\} \end{aligned} \tag{4.20}$$

Note that, both objective function and constraints of (P_3) are linear function of optimization parameters x_i. In the literature, this problem is known as the Binary Linear Program(BLP). BLP programs have applications in various areas including production planning, scheduling, cellular networks etc. These kind of optimization problems are known to be non-convex NP hard problems due to the integrality constraints and there is no known method for solving them in polynomial time. But, there are very powerful methods like linear programming based branch-and-bound algorithms that solve linear relaxations of integer programs by removing all the integrality constraints first then adding integrality constraint for each variable one by one. There is a large

literature on BLPs but details of these algorithms are not in the scope of this thesis and will not be given here.

In the following two sections, we will first explain how to handle $\{\phi_1, \phi_2\}$ pairs in set Υ. Then the modelling of sensor physical dimensions will discussed.

4.1.1 Determination of Azimuth Angles for Ambiguity Constraints

In previous section we showed that ambiguity constraints can be modelled as

$$T(\phi_1, \phi_2) \triangleq \sum_{i=2}^{m} x_i \cos\left(2\pi k_i(\cos\phi_2 - \cos\phi_1)\right) \leq \bar{T} \qquad \{\phi_1, \phi_2\} \in \Upsilon \tag{4.21}$$

where $\Upsilon \triangleq \{(\phi_1, \phi_2) \mid \phi_1 \in \Phi; \phi_2 \in \Phi; |\phi_1 - \phi_2| \geq \sigma\}$. Note that azimuth angle pairs closer than σ are discarded in the set Υ. As explained in chapter 3, errors for closely spaced angles are not considered as ambiguity. The parameter σ defines the smallest angle error that is considered as ambiguity and it also act as a parameter for adjusting the beamwidth of the beamformer. But still other constraints for beamwidth can also be added if desired.

Let γ be defined as

$$\gamma \triangleq cos(\phi_2) - cos(\phi_1) \tag{4.22}$$

In Fig. 4.3, values of γ is given for all azimuth angles in the interval $\Phi = [0, 180]$. Note that gamma just a continuous function of variable γ and it just maps the points in the set Υ into some limited interval $\Gamma \triangleq [\gamma_{min}, \gamma_{max}]$. In Fig. 4.2, relation between γ and $\{\phi_1, \phi_2\}$ is illustrated.

Substituting Eq. 4.22 into Eq. 4.21, we get

$$T(\gamma) \triangleq \sum_{i=2}^{m} x_i \cos\left(2\pi k_i \gamma\right) \leq \bar{T} \qquad \gamma \in \Gamma \tag{4.23}$$

Note that in Eq. 4.23, γ is inside an even function $\cos\left(2\pi k_i \gamma\right)$. So it is sufficient to consider either positive or negative values of γ. In Fig. 4.2, this corresponds to either one of the blue regions.

As we can not place constraints for infinite number of points in set Γ, we need to take sufficient number of samples between minimum and maximum values in set Γ. Con-

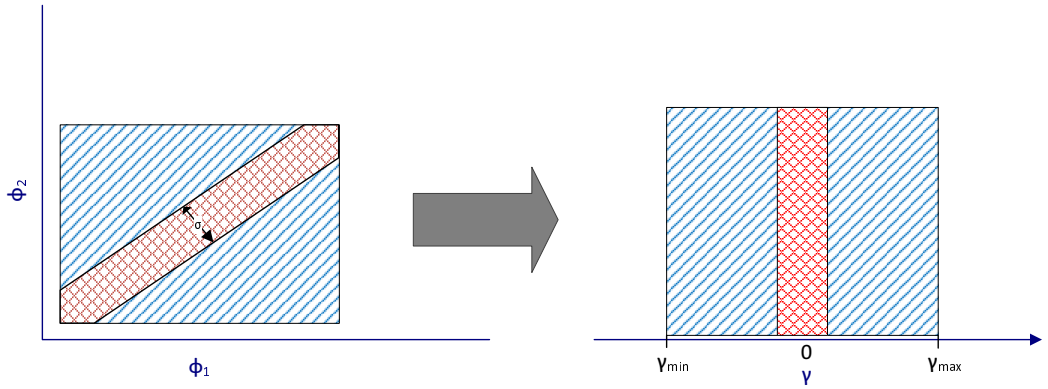

Figure 4.2: γ Mapping

sidering the even structure of function $T(\gamma)$, we calculate the minimum and maximum of values of gamma as follows,

$$\gamma_{min} = min(|\gamma(\phi_1, \phi_2)|) \qquad \{\phi_1, \phi_2\} \in \Upsilon \tag{4.24}$$

$$\gamma_{max} = max(|\gamma(\phi_1, \phi_2)|) \qquad \{\phi_1, \phi_2\} \in \Upsilon \tag{4.25}$$

Notice that, $\gamma(\phi_1, \phi_2)$ is a continuous function of ϕ_1, ϕ_2. So we can take sufficient number of samples between $[\gamma_{min}, \gamma_{max}]$ which is given by

$$\gamma[z] \triangleq \gamma_{min} + \frac{(\gamma_{max} - \gamma_{min})z}{Z-1} \qquad z = 1, 2, \ldots Z \tag{4.26}$$

where Z denotes the number γ samples and z denotes the sample index..

By using the samples of γ, we can write the Eq. 4.23 in matrix form as below.

$$\boldsymbol{A_1} = \begin{bmatrix} cos2\pi k_2\gamma_1 & cos2\pi k_3\gamma_1 & \cdots & cos2\pi k_m\gamma_1 \\ cos2\pi k_2\gamma_2 & cos2\pi k_3\gamma_2 & \cdots & cos2\pi k_m\gamma_2 \\ \vdots & \vdots & \vdots & \vdots \\ cos2\pi k_2\gamma_Z & cos2\pi k_3\gamma_Z & \cdots & cos2\pi k_m\gamma_Z \end{bmatrix} \tag{4.27}$$

$$\boldsymbol{A_1 x} = \begin{bmatrix} T(\gamma_1) \\ T(\gamma_2) \\ \vdots \\ T(\gamma_Z) \end{bmatrix} \tag{4.28}$$

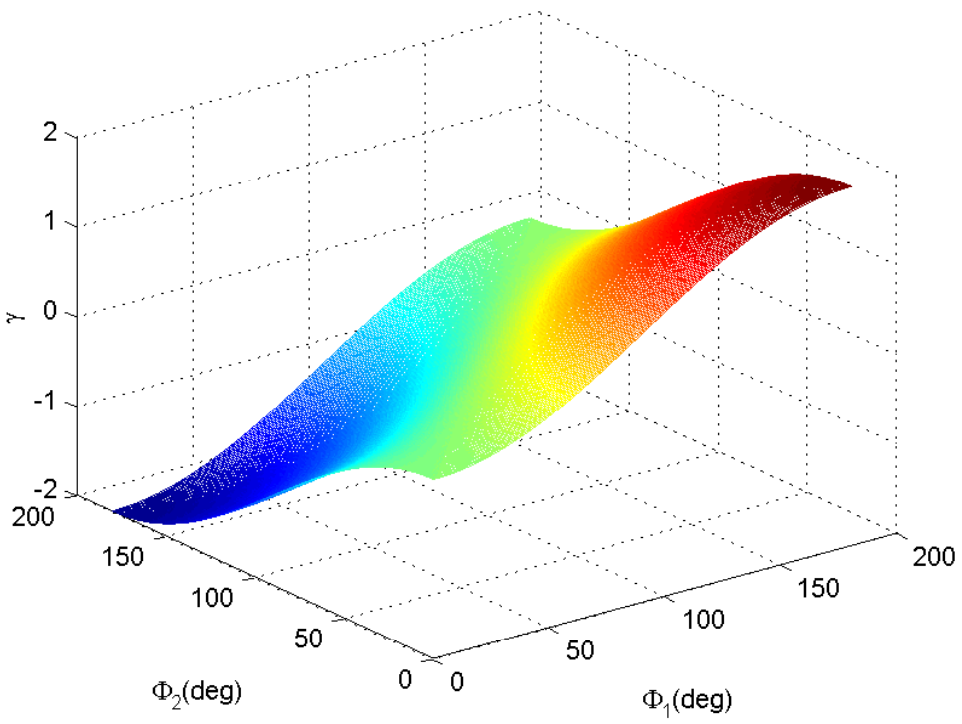

Figure 4.3: γ Values for $\Phi = [0, 180]$,$\sigma = 0$

As a result, we calculate the Z x (m-1) ambiguity constraint matrix where Z is the number ambiguity constraints and m is the number of sensors in the grid including the sensor on the origin.

Procedure for constructing the ambiguity constraint matrix is summarized in Algorithm 1.

Algorithm 1 Constructing Ambiguity Constraint Matrix

1: Construct the set Υ consisting of $\{\phi_1, \phi_2\}$ pairs using σ parameter and Φ given in Eq. 4.1

2: Compute $\gamma(\phi_1, \phi_2),\ \forall\{\phi_1, \phi_2\} \in \Upsilon$

3: $\gamma_{min} \leftarrow \min(|\gamma(\phi_1, \phi_2|)$

4: $\gamma_{max} \leftarrow \max(|\gamma(\phi_1, \phi_2|)$

5: Calculate $\gamma_z \triangleq \gamma_{min} + \frac{(\gamma_{max} - \gamma_{min})z}{Z-1} \qquad z = 1, 2, \ldots Z$ {Z is typically between 200 and 1000}

6: Compute A_1 given in Eq. 4.27 using sensor positions and γ_z values calculated in previous step.

4.1.2 Sensor Dimension Constraints

Especially for wideband sensors, sensor sizes might become very large compared to the wavelength in the maximum operating frequency. So ambiguities are very likely even if the sensors are placed with the minimum distance allowed by their sizes. But instead of placing them very close to each other, we can simply find sensor spacings that satisfy physical dimension constraints along with ambiguity constraints given in the previous section. One might think that instead of adding constraints to the optimization problem, minimum sensor spacing can be adjusted by increasing the sensor distances in the sensor grid. But this would decrease the number of different sensor spacings we could get and make it harder to satisfy the ambiguity constraints.

Integer constraints on sensor gains allow us to add physical dimensions of each sensor in the sensor grid as linear constraints to the original optimization problem. To do, this we define a vector for each sensor that has elements 1 for the positions occupied by the related sensor and 0 for the other positions in the sensor grid. We call this vector as the position mask of the related sensor. An example is illustrated in the Fig.4.4. For the given scenario, Sensor 1 and Sensor 2 cannot be used at the same time.

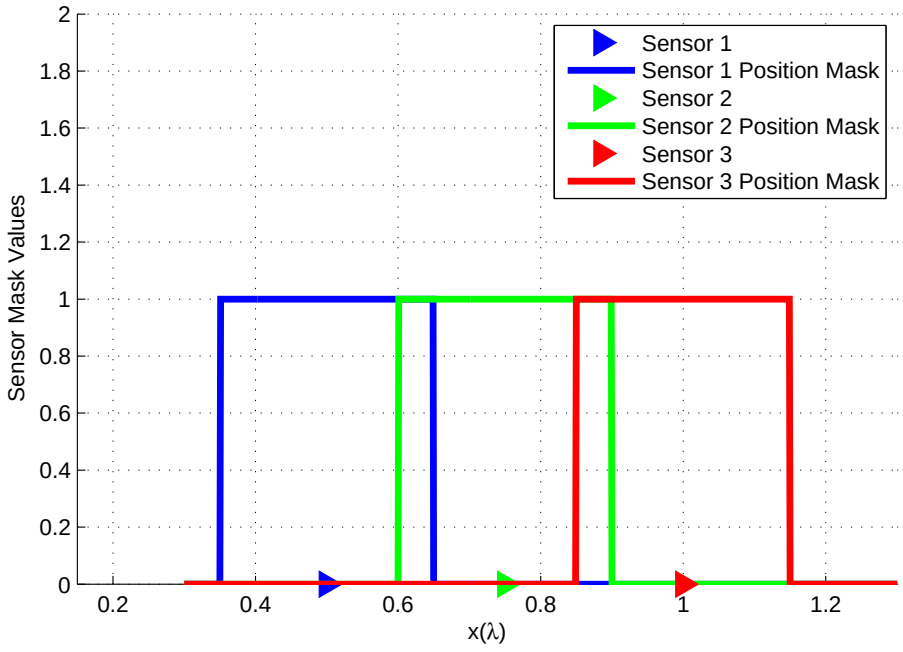

Figure 4.4: Sensor Dimension Constraints

Let $\boldsymbol{v}_i$ represent the (m-1)x1 position mask of the ith sensor in the grid excluding the sensor at the origin. Then we can write the sensor dimension constraint as follows.

$$\boldsymbol{v}_2 x_2 + \boldsymbol{v}_3 x_3 + \cdots + \boldsymbol{v}_m x_m \leq 1 \tag{4.29}$$

or in matrix form

$$\boldsymbol{A_2} \begin{bmatrix} x_2 \\ x_3 \\ \vdots \\ x_m \end{bmatrix} \leq 1 \tag{4.30}$$

where inequality shows element wise inequality and

$$\boldsymbol{A_2} \triangleq [\boldsymbol{v}_2 \ \boldsymbol{v}_3 \ \cdots \ \boldsymbol{v}_m] \tag{4.31}$$

It should not be forgotten that there is a sensor at the origin of the coordinate system all time. So this particular situation should be handled separately. One solution is to remove all the sensors in grid that blocks the sensor at the origin before starting the optimization.

For each sensor, position mask vector should be calculated for every sensor position in the grid. So it is a (m-1)x(m-1) matrix where m is the number of sensors in the grid including the sensor at the origin. Procedure for constructing sensor dimension constraint matrix is given in Algorithm 2.

Algorithm 2 Constructing Sensor Dimension Constraint Matrix

```
ki ← Positions of Sensors
m ← Number of Sensor in the grid {m variable in here does not include the sensor on the origin}
for SensorIndex = 1 to m do
    for PositionIndex = 1 to m do
        if Sensor at ki(SensorIndex) occupies position ki(PositionIndex) then
            A2(PositionIndex, SensorIndex) ← 1
        else
            A2(PositionIndex, SensorIndex) ← 0
        end if
    end for
end for
```

4.1.3 Linear Array Design Procedure

In sections 4.1.1 and 4.1.2, we explained how the constraint matrices should be computed for both ambiguity constraints and sensor dimension constraints. Now we are going to summarize the procedure of designing sensor arrays with worst case ambiguity probability that is lower than a given desired value and minimum sensor spacing compatible with the given sensor size. With the definitions made in sections 4.1.1 and 4.1.2, we can rewrite the optimization problem as

(P_4)

$$\begin{aligned} \underset{\mathbf{x}}{\text{minimize}} \quad & \|\mathbf{x}\|_1 \\ \text{subject to} \quad & \boldsymbol{A}_1\boldsymbol{x} \leq \tilde{T} \\ & \boldsymbol{A}_2\boldsymbol{x} \leq 1 \\ & \sum_{i=2}^{m} x_i \geq \tilde{Q} \\ & x_i \in \{0,1\} \qquad i = 2,3\ldots m \end{aligned} \tag{4.32}$$

where $\boldsymbol{A}_1$ holds for ambiguity constraints given in section 4.1.1 and $\boldsymbol{A}_2$ holds for sensor dimension constraint given in section 4.1.2.

Algorithm 3 Linear Unambiguous Array Design with Sensor Dimension Constraints

1: Form a linear grid of m sensors with maximum aperture size L as given in Fig. 4.1 and calculate their sensor positions
2: Define the angular sector of operation Φ given in Eq. 4.1
3: Choose the σ parameter considering the required array accuracy and resolution.{See Chapter 3 for further information}
4: Calculate the value $\bar{\beta}$ for the desired worst case ambiguity probability for a given SNR and number snapshots using the values of error function given Eq. 3.5
5: Determine minimum number of sensors(M) to be used.
6: $\bar{Q} \leftarrow M - 1$
7: $\bar{T} \leftarrow (M\bar{\beta} - 1)$
8: Calculate the ambiguity constraint matrix $\boldsymbol{A_1}$ as given in Algorithm 1
9: Calculate the sensor dimension constraint matrix $\boldsymbol{A_2}$ as given in Algorithm 2
10: Solve the optimization problem (P_4) given in Eq. 4.32
11: Determine the positions of sensors with non zero sensor gains as the sensor positions of the sparse array.

4.2 Multi Dimensional Array Geometries for 2D DOA Estimation

In the previous parts, we define an optimization problem for designing unambiguous linear arrays. Same method can readily be extended for arbitrary sensor grids in 3D space for 2D DOA estimation.

Let Φ and Θ denote the interval of operational azimuth and elevation angles of the sensor array.

$$\Phi \triangleq [\phi_{min}, \phi_{max}] \tag{4.33}$$

$$\Theta \triangleq [\theta_{min}, \theta_{max}] \tag{4.34}$$

Let Ψ denote the set of possible direction of arrivals, i.e,

$$\Psi \triangleq \{(\phi,\theta) \,|\phi \in \Phi, \theta \in \Theta\} \tag{4.35}$$

Consider a grid of sensors with arbitrary sensor locations. Steering vector with sensor gains for DOA $\psi \in \Psi$ is given by

$$\mathbf{g}(\psi) = [x_2 e^{j2\pi \boldsymbol{r}_2^T \boldsymbol{u}(\psi)}, x_3 e^{j2\pi \boldsymbol{r}_3^T \boldsymbol{u}(\psi)}, \cdots, x_m e^{j2\pi \boldsymbol{r}_m^T \boldsymbol{u}(\psi)}] \tag{4.36}$$

where $\boldsymbol{r}_i$ is the position vector containing x,y,z positions of the related sensors normalized with the wavelength and $\boldsymbol{u}(\psi)$ is the directional cosine vector for the direction $\psi \triangleq \{\phi, \theta\} \in \Psi$.

$$\boldsymbol{r}_i \triangleq [k_{x_i} \; k_{y_i} \; k_{z_i}]^T \tag{4.37}$$

$$\boldsymbol{u}(\psi) \triangleq [cos\phi sin\theta \; sin\phi sin\theta \; cos\theta]^T \tag{4.38}$$

Note that the set Ψ defines all the possible angle of arrivals in the operational range of the sensor array. So ambiguity constraints must be satisfied for all DOA combinations in the set Ψ, i.e,

$$T(\psi_1, \psi_2) \triangleq \Re\{\boldsymbol{g}(\boldsymbol{u}(\psi_1))^H \boldsymbol{g}(\boldsymbol{u}(\psi_1))\} = \sum_{i=2}^{m} x_i^2 \cos\left(2\pi \boldsymbol{r}_i^T \Delta\boldsymbol{u}\right) \leq \bar{T} \tag{4.39}$$

$$Q \triangleq \sum_{i=2}^{m} x_i \geq \bar{Q} \tag{4.40}$$

where $\psi_1 \in \Psi, \psi_2 \in \Psi$ and $\Delta\boldsymbol{u}$ defined as

$$\Delta\boldsymbol{u}(\psi_1, \psi_2) \triangleq \boldsymbol{u}(\psi_1) - \boldsymbol{u}(\psi_2) = \begin{bmatrix} cos\phi_1 sin\theta_1 - cos\phi_2 sin\theta_2 \\ sin\phi_1 sin\theta_1 - sin\phi_2 sin\theta_2 \\ cos\theta_1 - cos\theta_2 \end{bmatrix} \tag{4.41}$$

Let Υ denote the set consisting of (ψ_1, ψ_2) combinations where $\psi_1 \in \Psi, \psi_2 \in \Psi$. So for every $(\psi_1, \psi_2) \in \Upsilon$, we should add the ambiguity constraint using the Eq. 4.39. As we cannot add infinite number of constraints, we should define a method for selecting finite number of constraints just like we did in linear case where we define the variable γ given in Eq. 4.22. Only difference is, for linear array case we only have a variable γ for different direction of arrival combinations (ϕ_1, ϕ_2) whereas for 3D arrays, we have a 3×1 vector $\boldsymbol{\Delta u} \in \mathbb{R}^3$ given in Eq. 4.41.

In order to cast in a form similar to linear array case, we make the following definitions.

$$\gamma_1 \triangleq cos\phi_1 sin\theta_1 - cos\phi_2 sin\theta_2 \tag{4.42}$$

$$\gamma_2 \triangleq sin\phi_1 sin\theta_1 - sin\phi_2 sin\theta_2 \tag{4.43}$$

$$\gamma_3 \triangleq cos\theta_1 - cos\theta_2 \tag{4.44}$$

So $\boldsymbol{\Delta u}$ given in Eq. 4.41 becomes

$$\boldsymbol{\Delta u}(\psi_1, \psi_2) = \begin{bmatrix} \gamma_1 \\ \gamma_2 \\ \gamma_3 \end{bmatrix} \tag{4.45}$$

Note that values of $\gamma_1, \gamma_2, \gamma_3$ are induced by the set Υ. Depending on the operational angles of the array, intervals of γ_i will change. We can use a method similar to linear array case for defining all the $\boldsymbol{\Delta u}$ that are to be used when calculating the ambiguity constraint matrix. The intervals of γ_i can be calculated for the array operational range as follows.

$$\Gamma_1 \triangleq [\gamma_{1_{min}}, \gamma_{1_{max}}] \tag{4.46}$$

$$\Gamma_2 \triangleq [\gamma_{2_{min}}, \gamma_{2_{max}}] \tag{4.47}$$

$$\Gamma_3 \triangleq [\gamma_{3_{min}}, \gamma_{3_{max}}] \tag{4.48}$$

In order to have better understanding, we can use an example to show how to choose the ambiguity constraints. We assume that we have a grid of sensors on x-z plane for 2D DOA estimation. As it can be easily seen from the Eq. 4.39, for sensors on x-z plane, we should only consider the values of γ_1 and γ_3. Let the azimuth operational

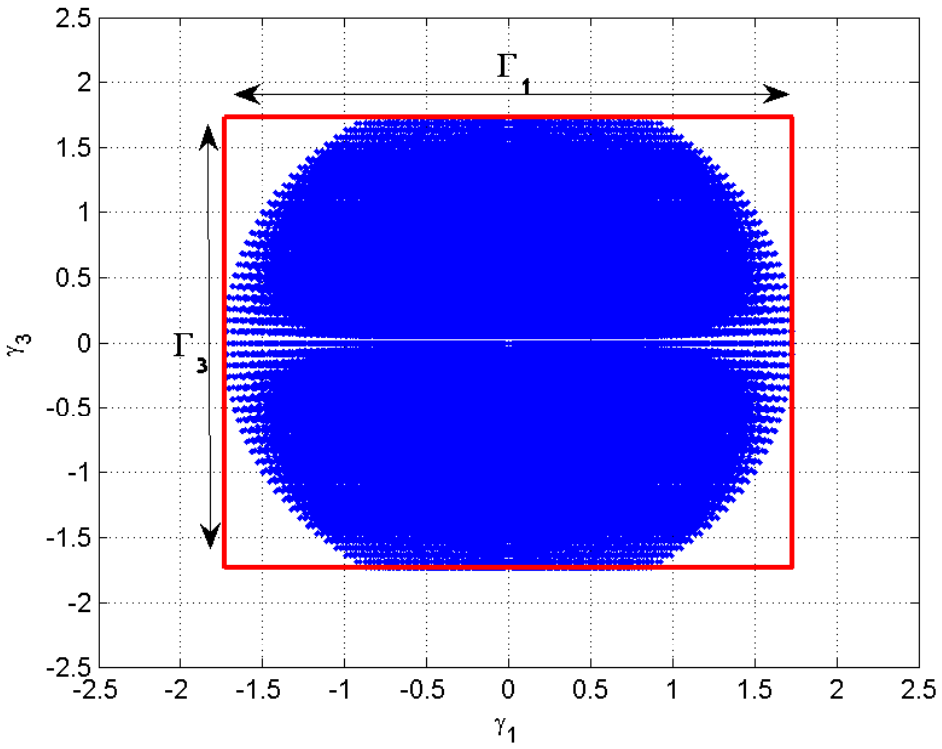

Figure 4.5: Values of γ_1 and γ_3 for $\Phi = [30, 150]$ and $\Theta = [30, 150]$

range be $\Phi = [30, 150]$ and elevation operational range be $\Theta = [30, 150]$. In Fig. 4.5, values of γ_1 and γ_3 is illustrated. By taking sufficient samples in the intervals Γ_1 and Γ_3, we can form the ambiguity constraint points as given below.

$$\gamma_1[z] \triangleq \gamma_{1_{min}} + \frac{(\gamma_{1_{max}} - \gamma_{1_{min}})z}{Z_1 - 1} \qquad z = 1, 2, \ldots Z_1 \tag{4.49}$$

$$\gamma_3[z] \triangleq \gamma_{3_{min}} + \frac{(\gamma_{3_{max}} - \gamma_{3_{min}})z}{Z_3 - 1} \qquad z = 1, 2, \ldots Z_3 \tag{4.50}$$

where Z_i denotes the number of γ_i samples.

Note that the minimum value of γ_1 is dependent on the value of γ_3 in Fig. 4.5. By choosing the ambiguity points as in Eq. 4.49 and Eq. 4.50 we place uniformly distributed constraints inside the region defined by the red lines in Fig. 4.5. By doing so we place constraints to some points that we actually do not have to. Eliminating these points is not necessary and optimization problem can still be solved. But by eliminating them we can have less number of constraints which decreases the solution time of the problem and also increases the probability of finding a feasible solution.

After forming the constraint points, we still need to eliminate the closely spaced direc-

tion of arrivals as we did for linear array case. Note that the norm of the $\Delta \boldsymbol{u}$ given in Eq. 4.45 becomes 0 as the direction of arrivals ψ_1, ψ_2 gets close to each other. So by eliminating the $\Delta \boldsymbol{u}$ vectors with small norm we can eliminate the constraints belonging to closely separated direction of arrivals.

$$\|\Delta \boldsymbol{u}\|^2 = \gamma_1^2 + \gamma_2^2 + \gamma_3^2 \leq \epsilon \tag{4.51}$$

where ϵ is related to the desired beamwidth of the beamformer. By increasing the ϵ value, we actually decrease the number of constraint we place and increase the beamwidth of the beamformer. As ϵ decreases, we place constraint for smaller angle separations and narrow the beamwidth of the beamformer hence increase the accuracy of the sensor array.

DOA accuracy of both elevation and azimuth angle estimates can be controlled independently by weighting the γ_i terms in Eq. 4.51 as below.

$$a\gamma_1^2 + b\gamma_2^2 + c\gamma_3^2 \leq \epsilon \tag{4.52}$$

In Fig. 4.6, we demonstrate the elimination of closely separated angles for the planar array on x-z plane with the constraints given in Fig 4.5.

It should be noted that there might be different approaches for eliminating the constraints for closely separated angles and we just give a one way of doing it. Depending on the application and requirements of the array, different approaches can be derived.

We can write the ambiguity constraints in matrix form just similar to the linear case as below. Ambiguity constraint matrix is given by

$$\mathbf{A}_1 = \begin{bmatrix} cos(2\pi \boldsymbol{r}_2^T \Delta \boldsymbol{u}_1) & cos(2\pi \boldsymbol{r}_3^T \Delta \boldsymbol{u}_1) & \cdots & cos(2\pi \boldsymbol{r}_m^T \Delta \boldsymbol{u}_1) \\ cos(2\pi \boldsymbol{r}_2^T \Delta \boldsymbol{u}_2) & cos(2\pi \boldsymbol{r}_3^T \Delta \boldsymbol{u}_2) & \cdots & cos(2\pi \boldsymbol{r}_m^T \Delta \boldsymbol{u}_2) \\ \vdots & \vdots & \vdots & \vdots \\ cos(2\pi \boldsymbol{r}_2^T \Delta \boldsymbol{u}_{Z_T}) & cos(2\pi \boldsymbol{r}_3^T \Delta \boldsymbol{u}_{Z_T}) & \cdots & cos(2\pi \boldsymbol{r}_m^T \Delta \boldsymbol{u}_{Z_T}) \end{bmatrix} \tag{4.53}$$

$$\boldsymbol{A_1 x} = \begin{bmatrix} T(\Delta \boldsymbol{u}_1) \\ T(\Delta \boldsymbol{u}_2) \\ \vdots \\ T(\Delta \boldsymbol{u}_{Z_T}) \end{bmatrix} \tag{4.54}$$

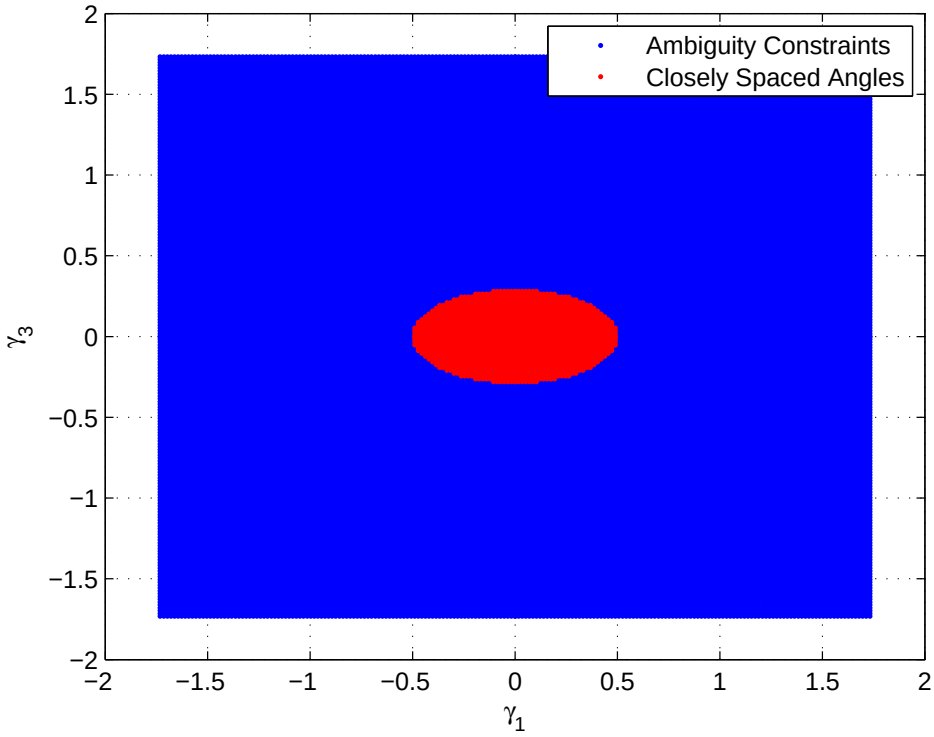

Figure 4.6: Elimination of closely spaced angles, $a = 2, b = 6, \epsilon = 0.5$

where Z_T is the total number of ambiguity constraints in $\mathbb{R}^3$.

Sensor dimension constraints are also be extended for 3D arrays. The method given in section 4.1.2 is directly applicable for 3D arrays.

A brief summary for designing sensor arrays for 2D DOA estimation is summarized in Algorithm 4.

Algorithm 4 3D Unambiguous Array Design for 2D DOA Estimation

1: Form a multidimensional sensor array in 3D space
2: Define the azimuth angular sector of operation Φ given in Eq. 4.33 and elevation angular sector of operation Θ given in Eq. 4.34.
3: Choose the parameters a, b, c and ϵ parameters considering the required array accuracy and resolution.
4: Calculate the value $\bar{\beta}$ for the desired worst case ambiguity probability for a given SNR and number snapshots using the values of error function given Eq. 3.5
5: Determine minimum number of sensors(M) to be used.
6: $\bar{Q} \leftarrow M - 1$
7: $\bar{T} \leftarrow (M\bar{\beta} - 1)$
8: Calculate the ambiguity constraint matrix $\boldsymbol{A_1}$ as given in Eq. 4.53.
9: Calculate the sensor dimension constraint matrix $\boldsymbol{A_2}$ as given in Algorithm 2
10: Solve the optimization problem (P_4) given in Eq. 4.32
11: Determine the positions of sensors with non zero sensor gains as the sensor positions of the sparse array.

4.3 Finding the Sparsest Array by Iteratively Launching the Optimization Problem

As it is stated before, by adding the constraint given in Eq. 4.18, minimum number of sensors to be used is lower bounded by the value $\bar{Q} + 1$. So depending on the value of the $\bar{Q}$, we might only be able to find a sparse array that is not the sparsest possible. To overcome this situation, we can launch the optimization problem given in Eq. 4.32 to find the sparsest array. Starting with $\bar{Q} = 1$, we first try to find a sensor array with two sensors that satisfy all the constraints. In every iteration we increase the minimum number of sensors until the solver finds a feasible solution. While doing this, we must also update the variable $\bar{T}$ to satisfy the same worst case ambiguity probability. Iterations are stopped when a feasible solution is found.

In Algorithm 5, we summarize the method for sparsest array design.

Algorithm 5 Sparsest Sensor Array Design by Iteratively Launching Binary Linear Program

1: //Initialize
2: Form a linear grid of m sensors with maximum aperture size L as given in Fig. 4.1 and calculate their sensor positions
3: Define the angular sector of operation Φ given in Eq. 4.1
4: Choose the σ parameter considering the required array accuracy and resolution.{See Chapter 3 for further information}
5: Calculate the value $\bar{\beta}$ for the desired worst case ambiguity probability for a given SNR and number snapshots using the values of error function given Eq. 3.5
6: Calculate the ambiguity constraint matrix $\boldsymbol{A_1}$ as given in Algorithm 1
7: Calculate the sensor dimension constraint matrix $\boldsymbol{A_2}$ as given in Algorithm 2
8: $\bar{Q} \leftarrow 1$
9: **repeat**
10: $\quad \bar{Q} \leftarrow \bar{Q} + 1$
11: $\quad \bar{T} \leftarrow (M\bar{\beta} - 1)$
12: $\quad$ Solve the optimization problem given in Eq. 4.32.
13: **until** (A Feasible Solution is Found)

CHAPTER 5

SIMULATIONS AND RESULTS

In this chapter, we provide some examples in order to demonstrate the ability of designing linear and planar arrays using the method we proposed in previous sections. In order to solve the optimization problem given in Eq. 4.32, CVX[22] and one of the commercial solvers, Gurobi[23], are used together in Matlab environment. In order to show the effects of parameters used during the design procedure, different arrays are designed. All sensor positions are given in units of wavelength so sensor positions should be scaled with maximum frequency of operation.

5.1 Linear Array Design Examples

5.1.1 Experiment 1

First, we design two different linear arrays with different design criterions. Parameters used for each design are given in Table 5.1.

Table5.1: Design Parameters for Linear Arrays

Parameters	**Array 1**	**Array 2**
$\Phi(degrees)$	[30, 150]	[30, 150]
$\sigma(degrees)$	2	7
$MaximumAperture(\lambda)$	20	10
$GridSpacing(\lambda)$	0.01	0.01
m(# of Sensors in the Grid)	2001	1001
M(Minimum # of Sensors to be Used)	4	4
T	2.5	2.5
Worst-Case $B(\phi_1, \phi_2)$	0.875	0.875
Worst-Case P_a for 0 dB SNR, 100 Snapshots	5.737e-7	5.737e-7
Sensor Size(λ)	1.8	1.5
# of Ambiguity Constraints	200	200

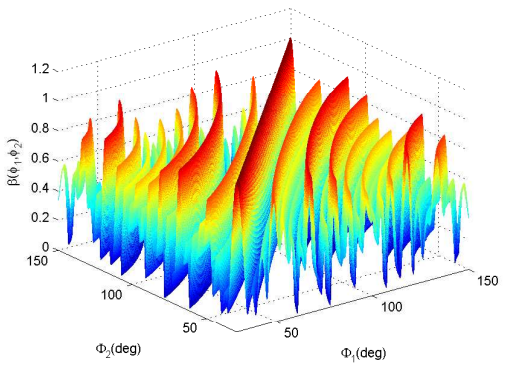

(a) $\beta(\phi_1, \phi_2)$ for Array 1

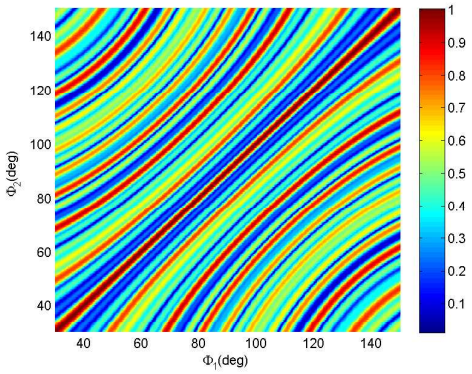

(b) $\beta(\phi_1, \phi_2)$, for Array 1, Top View

Figure 5.1: $\beta(\phi_1, \phi_2)$ for Array 1

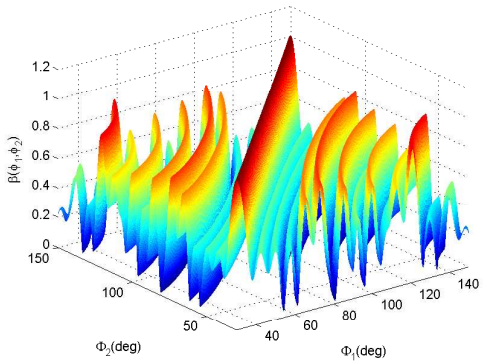

(a) $\beta(\phi_1, \phi_2)$ for Array 2

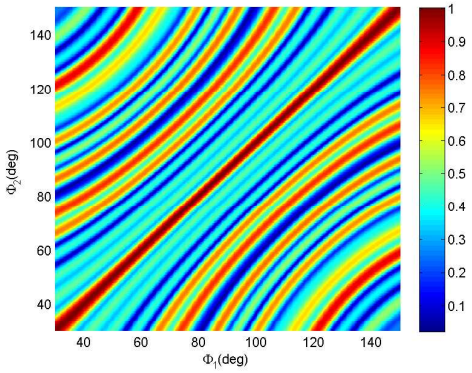

(b) $\beta(\phi_1, \phi_2)$, for Array 2, Top View

Figure 5.2: $\beta(\phi_1, \phi_2)$ for Array 2

In Fig. 5.1 and 5.2, ambiguity related function $\beta(\phi_1, \phi_2)$ for both arrays is given. Comparing the β functions of both arrays we see that beamwidth of the Array 1 is narrower than beamwidth of the Array 2. This was the expected result considering the σ parameters of both arrays given in Table 5.1. By choosing a lower value for σ for Array 1, we actually desired a better accuracy and resolution. As a result, we get a larger aperture for Array 1 and ambiguity conditions are still satisfied.

Monte Carlo simulations are done for both arrays in order to see the array estimation performance for single source case. During the simulations, measurements are generated uniformly spaced angles in the operational range Φ of the arrays given in Table 5.1. In Table 5.3, array positions for both arrays are also given. During the accuracy experiments, Spectral MUSIC algorithm is used as the DOA estimator and

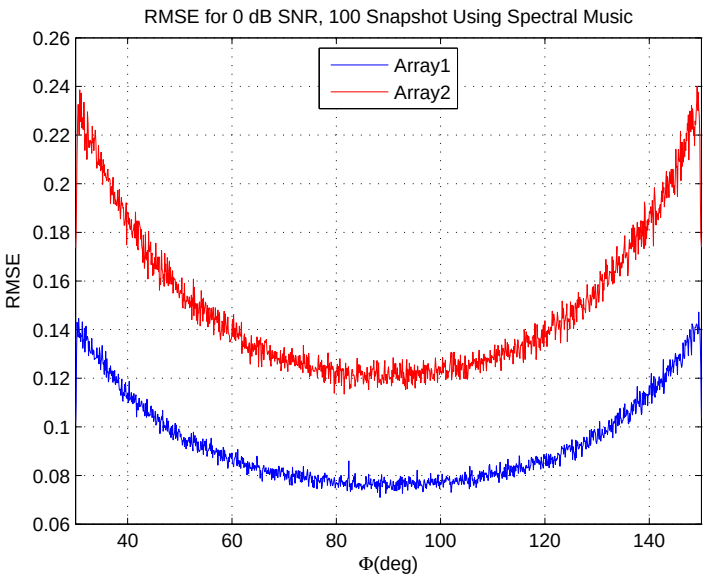

Figure 5.3: RMSE for Array 1

it is assumed that number of sources is known. All experiment parameters are given in Table 5.2.

In Fig. 5.3, estimation performance of both arrays are shown. It can be seen that, RMSE of DOA estimation increases when the target moves away from the boresight angle. This is an expected result due to the characteristics of the linear array. As the target moves away from the boresight, effective aperture of the arrays decreases. This can also be observed just by checking the Fig. 5.1 and Fig. 5.2. Note that, as the steering angle of the beamformer moves away from the boresight, beamwidth increases.

Table5.2: Monte Carlo Experiment Parameters

Parameters	**Value**
SNR(dB)	20
Snapshots	100
AOA Angle Resolution for Measurement(deg)	0.1
Spectral Music Search Angle Resolution(deg)	0.1
# of Monte Carlo Runs	1000

Table5.3: Sensor Positions of Array 1 and Array 2

Array 1	**Array 2**
x(λ)	x(λ)
0	0
-4.36	-4.95
-3.88	-1.59
9.77	3.73

5.1.2 Experiment 2

In this part, we give two linear array examples to see the effect of sensor dimension sizes. Two linear arrays with the parameters given in Table 5.4 are designed.

Table5.4: Design Parameters for Linear Arrays

Parameters	**Array 1**	**Array 2**
$\Phi(degrees)$	[30, 150]	[30, 150]
$\sigma(degrees)$	20	20
$MaximumAperture(\lambda)$	10	10
$GridSpacing(\lambda)$	0.01	0.01
m(# of Sensors in the Grid)	1001	1001
M(Minimum # of Sensors to be Used)	5	5
$\bar{T}$	3	3
Worst-Case $B(\phi_1, \phi_2)$	0.8	0.8
Worst-Case P_a for 0 dB SNR, 100 Snapshots	6.421e-10	6.421e-10
Sensor Size(λ)	1.5	1.8
# of Ambiguity Constraints	1000	1000

In Table 5.5, we give the element positions for both arrays. It can be seen that both arrays have 5 elements and optimum solution of the problem is found. For Array 1, we have the minimum sensor spacing 1.57λ whereas for Array 2, minimum spacing is 1.81λ. It seems that sensor dimension constraints are satisfied for both arrays.

In Fig. 5.4, ambiguity related function $\beta(\phi_1, \phi_2)$ is given for both sensor arrays.

Table5.5: Sensor Positions of Array 1 and Array 2

Array 1	**Array 2**
x(λ)	x(λ)
0	0
-4.55	-4.96
-2.98	-3.15
2.61	2.44
4.8	4.61

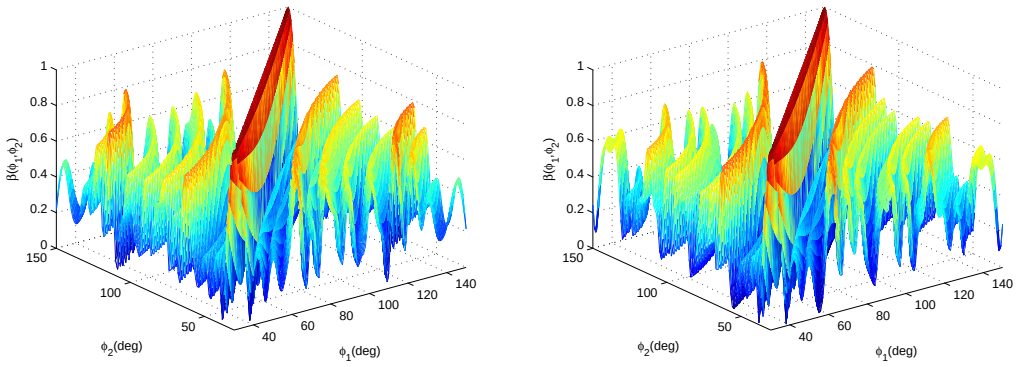

(a) $\beta(\phi_1, \phi_2)$ for Array 1

(b) $\beta(\phi_1, \phi_2)$, for Array 2

Figure 5.4: $\beta(\phi_1, \phi_2)$ for Array 1

5.1.3 Experiment 3

In experiment 3, we design a linear with 180 degree azimuth coverage. Array design parameters are given in Table 5.6. In Table 5.7, sensor positions of the array are given.

Note that 6 element sensor array has almost 20λ baseline. Uniform Linear Array with six elements would have 3λ baseline in order to have unambiguous response. By using our method, we have almost 6 times large aperture resulting in a narrower beamwidth and superior performance.

In Fig. 5.5, ambiguity related function is given for the sensor positions given in the Table 5.7.

Table5.6: Design Parameters for Linear Arrays

Parameters	**Array 1**
$\Phi(degrees)$	[0, 180]
$\sigma(degrees)$	20
$MaximumAperture(\lambda)$	20
$GridSpacing(\lambda)$	0.01
m(# of Sensors in the Grid)	2001
M(Minimum # of Sensors to be Used)	6
$\bar{T}$	3.8
Worst-Case $B(\phi_1, \phi_2)$	0.8
Worst-Case P_a for 0 dB SNR, 100 Snapshots	6.421e-10
Sensor Size(λ)	1.5
# of Ambiguity Constraints	1000

Table5.7: Sensor Positions of the Array with 180 Azimuth Coverage

$x_1(\lambda)$	$x_2(\lambda)$	$x_3(\lambda)$	$x_4(\lambda)$	$x_5(\lambda)$	$x_6(\lambda)$
0	-9.93	-7.36	-1.85	6.52	9.58

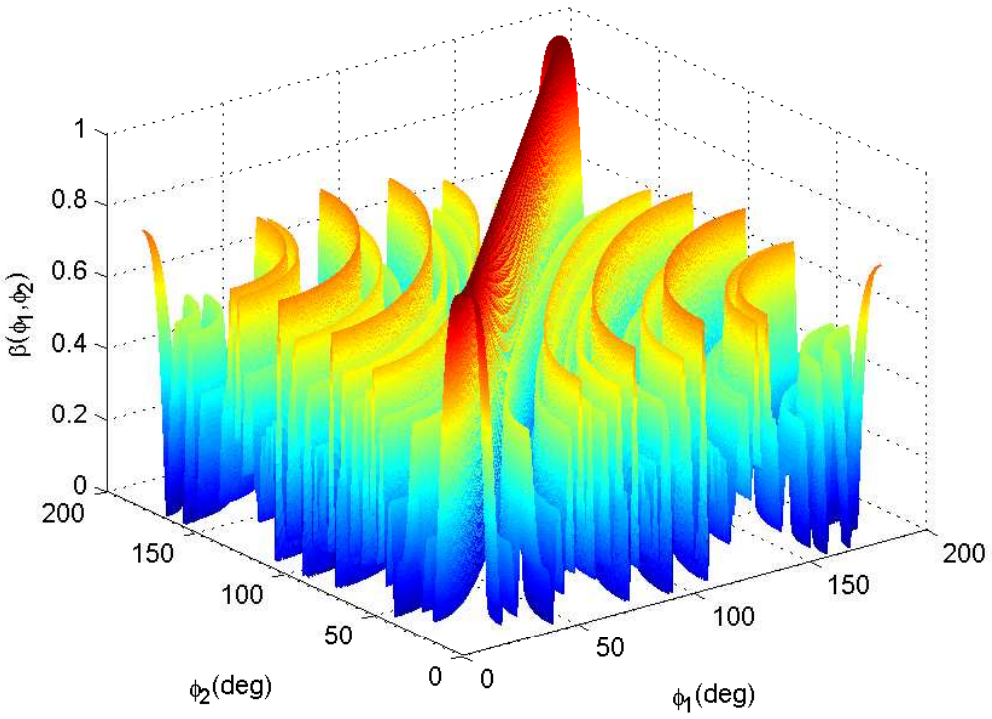

Figure 5.5: Ambiguity Related Function of the Sensor Array

5.1.4 Experiment 4

In experiment 4, we illustrate the ability of designing sensor arrays with minimum number of elements using the iterative approach proposed in Section 4.3. Design specifications that should be satisfied by the sensor array are given in Table 5.8.

Table5.8: Design Parameters for Linear Array with Minimum Number of Elements

Parameters	**Array 1**
$\Phi(degrees)$	[0, 180]
$\sigma(degrees)$	20
$MaximumAperture(\lambda)$	10
$GridSpacing(\lambda)$	0.01
m(# of Sensors in the Grid)	1001
Worst-Case $B(\phi_1, \phi_2)$	0.8
Worst-Case P_a for 0 dB SNR, 100 Snapshots	6.421e-10
Sensor Size(λ)	1.8
# of Ambiguity Constraints	1000

Using the parameters given in Table 5.8, iterative optimization problem is solved as given in Algorithm 5 and solution with 5 sensors is found. In Fig. 5.6, ambiguity related function is given for the designed sensor array. Sensor positions for the array are given in Table 5.9.

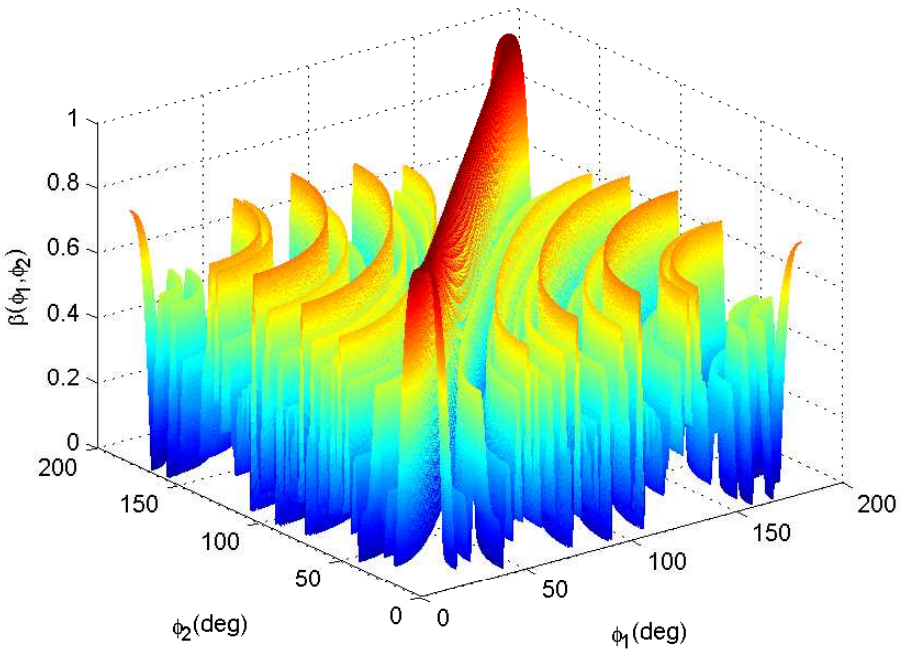

Figure 5.6: Ambiguity Related Function of the Sensor Array

Table5.9: Sensor Positions for Linear Array with Minimum Number of Elements

$x_1(\lambda)$	$x_2(\lambda)$	$x_3(\lambda)$	$x_4(\lambda)$	$x_5(\lambda)$
0	-4.5	-2.4	3.02	4.83

5.2 Planar Array Designs for 2D Direction Finding

In this part we demonstrate the ability of designing planar arrays for 2D direction finding. Design parameters used during design process for two different arrays are given in Table 5.10. It is assumed that arrays are on the xz plane. Main difference between the both arrays is the elevation coverage. Array 2 has a larger coverage for elevation direction finding.

During the computing of the sensor dimension constraint matrix, it is assumed that sensors are rectangles with the dimensions given in the Table 5.10.

Table5.10: Design Parameters for Planar Arrays

Parameters	**Array 1**	**Array 2**
Ψ	[30, 150]	[30, 150]
Θ	[60, 120]	[30, 150]
Maximum Aperture in x Dimension(λ)	5	5
Maximum Aperture in z Dimension(λ)	5	5
Grid Spacing in x Dimension(λ)	0.1	0.1
Grid Spacing in z Dimension(λ)	0.25	0.25
m(# of Sensors in the Grid)	1071	1071
M(Minimum # of Sensors to be Used)	5	5
$\bar{T}$	3.2	3.2
Sensor Size in x Dimension(λ)	1.5	1.5
Sensor Size in z Dimension(λ)	1	1
# of Ambiguity Constraints	40000	40000

In Table 5.11, sensor positions of both arrays are given in units of wavelength whereas in Fig.5.7, sensor positions for each array are illustrated. It can be seen that both arrays have 5 elements and solutions with minimum number of sensors in Table 5.10 are found.

Table5.11: Sensor Positions of 2D Arrays

Array 1			**Array 2**		
x(λ)	y(λ)	z(λ)	x(λ)	y(λ)	z(λ)
0	0	0	0	0	0
-1.6	0	0.25	-1.5	0	-0.25
-1	0	2	-1.1	0	1.25
-0.7	0	-2.5	0.1	0	-1.5
1.5	0	-2	1.5	0	1.25

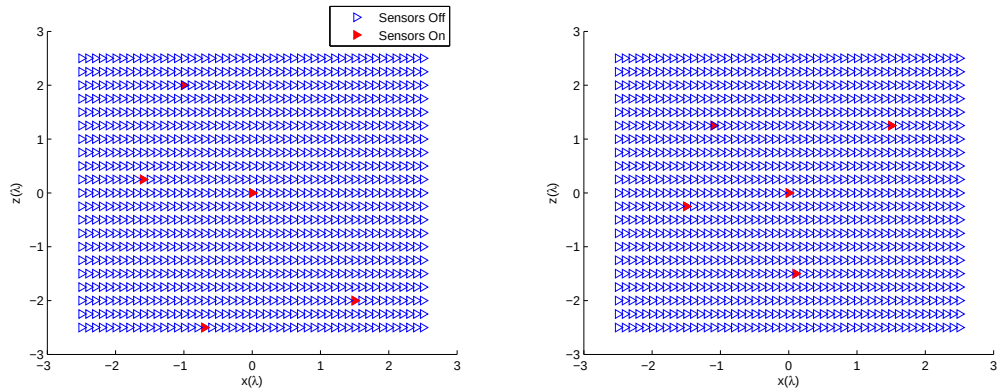

(a) Element Positions for Array 1

(b) Element Positions for Array 2

Figure 5.7: Element Positions for Array 1 and Array 2

Monte Carlo experiments are made in order to see the DF accuracy of both arrays. Experiment parameters are given in Table 5.12. Target AOA is changed uniformly in the sets Φ and Θ given in Table 5.10 for both arrays.

Table5.12: Monte Carlo Experiment Parameters for Planar Arrays

Parameters	**Value**
SNR(dB)	20
Snapshots	100
Azimuth AOA Angle Resolution for Measurement(deg)	2
Elevation AOA Angle Resolution for Measurement(deg)	2
Spectral Music Search Angle Resolution(deg)(Azimuth)	1
Spectral Music Search Angle Resolution(deg)(Elevation)	1
# of Monte Carlo Runs	1000

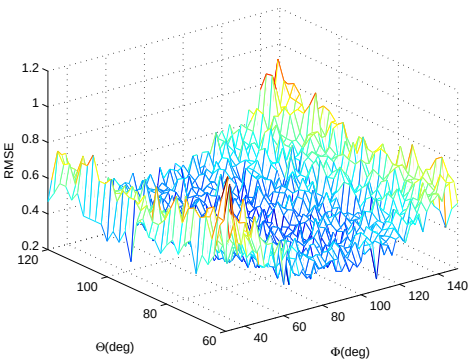

(a) Azimuth RMSE for Array 1

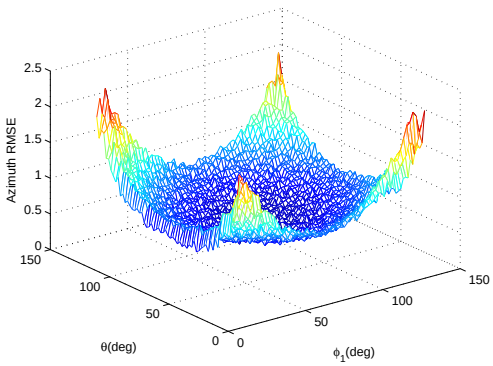

(b) Azimuth RMSE Array for Array 2

Figure 5.8: Azimuth DOA Estimation Accuracy for Both Arrays

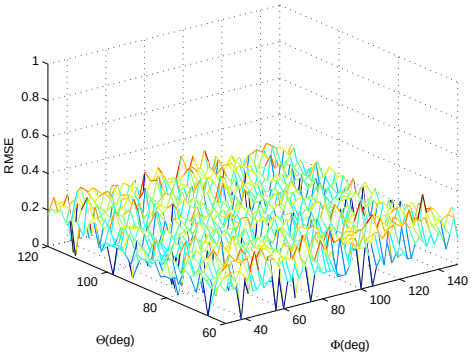

(a) Elevation RMSE for Array 1

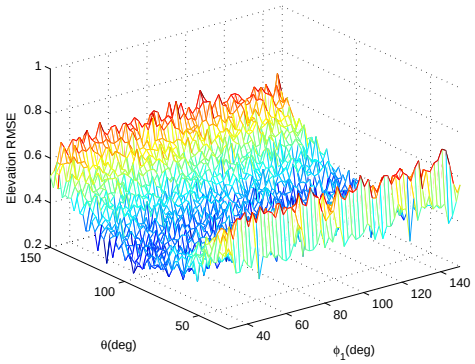

(b) Elevation RMSE Array for Array 2

Figure 5.9: Elevation DOA Estimation Accuracy for Both Arrays

In Fig. 5.8 and 5.9, estimation accuracy for azimuth and elevation are given. Similar to linear array results, these arrays perform best for targets at their boresight.

CHAPTER 6

CONCLUSIONS

In this thesis, a new approach is proposed for designing sparse sensor arrays that are to be used in direction finding applications. For sparse arrays, ambiguity problem should be considered during the design process of the array geometry. To achieve this purpose, we first investigated the relation with the array geometry and ambiguity problem. It is known that the probability of choosing the wrong DOA is related to the function of steering vectors and SNR. Further studies reveal that ambiguity related function does not only determine the ambiguity response of the array but also affects the estimation accuracy and resolution of the sensor array. Therefore ambiguity related function constituted a basis for our design approach.

In this work, sensor array design problem with unambiguous response is modelled as a binary linear program. Binary linear programs are known to be non convex and NP hard due to the integer constraints and there is no known method for solving them in polynomial time. But there are very powerful methods and algorithms that could find the optimum solution of these kinds of problems in a very efficient manner given that a feasible solution exist. Simulations show that sensors arrays could be designed with the proposed approach in a very fast manner.

In order to form the optimization problem, we first introduced binary sensor gains into the steering vectors and this helps us to transform the problem from determining the sensor positions to finding the sparse sensor gain vector. Then worst case ambiguity probability is added as linear constraints to the optimization problem by using an approximation of the ambiguity related function. Using the same approximation of the ambiguity related function, we also placed constraints for the required DOA accuracy

and resolution.

Practical design constraints have been studied as well. In most practical applications, sensors are large compared to the wavelength and it is not always possible to place them as desired. Also there are different placement requirements especially for moving platforms. Constraints related to the sensor sizes are modelled as a linear function of sensor gains and used as the constraints of the optimization problem. Also by forming the starting sensor positions properly, arbitrary shaped arrays can be designed including 3D and conformal arrays.

Our approach has numerous advantages compared to the methods in the array design literature. None of the methods in the literature offers the same degree of flexibility provided by our approach. First of all, our design approach is applicable for sensor arrays in 3D dimension for both azimuth and elevation DOA estimation. Using the proposed method, one can directly control the sparsity, ambiguity response, accuracy and sensor sizes of the sensor array. All of these requirements are handled inherently by the optimization problem defined in Eq.4.32. And also by casting the problem in a known optimization problem form, our approach finds the solution as a result of systematic search not brute force. For example, in [5], authors propose a method for finding the array with lowest ambiguity probability in a given set of possible candidates. To do this, they use a tight lower bound for their similarity measure and calculate this lower bound for every array candidate. Although calculated bound makes it easy to search for the best array, the problem becomes a very hard problem when number of arrays is large. Also there is no guarantee that the found array geometry will satisfy the desired ambiguity response or not.

Main disadvantage of the given approach is that optimization problem given in Eq.4.32 has a constraint that lower bounds the minimum number of sensors in the solution. So every time we launch the optimization problem, it will find the array with at least given minimum number of elements which might not be the optimal sparse array for the given ambiguity and other constraints. As we would like to find the sparsest array, it is not desired to limit the minimum number of sensors to be used. But results given in chapter 5 show that found arrays are indeed very sparse. Another disadvantage is that, there is no known method to understand if the optimization problem given in

Eq.4.32 is feasible for the given set of constraints.

In chapter 5, we provided some results for different scenarios. Results support that proposed approach can find sensor positions for the given design parameters in an efficient manner. It is shown that, by choosing the correct design parameters of the optimization problem given in Eq.4.32, one can design different shaped arrays that satisfy worst case ambiguity probability and required DOA accuracy. For example, when we choose a narrower beamwidth, proposed method tends to place the sensors so that array has a baseline large enough to satisfy the required accuracy.

As a future work, determination of ambiguity constraint points could be further investigated. By simplifying the method used for determining the ambiguity constraint points for 2D DOA estimation, we might be able to reduce the number of ambiguity constraints. Especially for 3D case, this would help us to design larger sensor arrays. Moreover, different constraints for DOA accuracy could be implemented. For example, constant beamwidth constrain for all steering angles of the beamformer could be used for omnidirectional(i.e, constant with respect to AOA) accuracy.

REFERENCES

[1] T Engin Tuncer and Benjamin Friedlander. *Classical and modern direction-of-arrival estimation*. Access Online via Elsevier, 2009.

[2] Houcem Gazzah. Optimum antenna arrays for isotropic direction finding. *Aerospace and Electronic Systems, IEEE Transactions on*, 47(2):1482–1489, 2011.

[3] Emest Jacobs and EW Ralston. Ambiguity resolution in interferometry. *Aerospace and Electronic Systems, IEEE Transactions on*, (6):766–780, 1981.

[4] Lal C Godara and Antonio Cantoni. Uniqueness and linear independence of steering vectors in array space. *The Journal of the Acoustical Society of America*, 70:467, 1981.

[5] Motti Gavish and Anthony J Weiss. Array geometry for ambiguity resolution in direction finding. *Antennas and Propagation, IEEE Transactions on*, 44(6):889–895, 1996.

[6] M Gavish and AJ Weiss. Array geometry optimization for ambiguity resolution in direction finding. In *Electrical and Electronics Engineers in Israel, 1995., Eighteenth Convention of*, pages 5–2. IEEE, 1995.

[7] CW Helstrom. The resolution of signals in white gaussian noise. *Proceedings of the IRE*, 43(9):1111–1118, 1955.

[8] Harry L Van Trees. *Detection, Estimation, and Modulation Theory, Optimum Array Processing*. John Wiley & Sons, 2004.

[9] Steven M Kay. *Fundamentals of Statistical signal processing, Volume 2: Detection theory*. Prentice Hall PTR, 1998.

[10] Ralph Schmidt. Multiple emitter location and signal parameter estimation. *Antennas and Propagation, IEEE Transactions on*, 34(3):276–280, 1986.

[11] Ilan Ziskind and Mati Wax. Maximum likelihood localization of multiple sources by alternating projection. *Acoustics, Speech and Signal Processing, IEEE Transactions on*, 36(10):1553–1560, 1988.

[12] Harald Cramér. *Mathematical Methods of Statistics (PMS-9)*, volume 9. Princeton university press, 1999.

[13] Ulkü Oktel and Randolph L Moses. A bayesian approach to array geometry design. *Signal Processing, IEEE Transactions on*, 53(5):1919–1923, 2005.

[14] Hagit Messer. Source localization performance and the array beampattern. *Signal processing*, 28(2):163–181, 1992.

[15] Kristine L Bell, Yariv Ephraim, and Harry L Van Trees. Explicit ziv-zakai lower bound for bearing estimation. *Signal Processing, IEEE Transactions on*, 44(11):2810–2824, 1996.

[16] Alon Amar and Anthony J Weiss. Fundamental limitations on the resolution of deterministic signals. *Signal Processing, IEEE Transactions on*, 56(11):5309–5318, 2008.

[17] Mostafa Kaveh and Ai Barabell. The statistical performance of the music and the minimum-norm algorithms in resolving plane waves in noise. *Acoustics, Speech and Signal Processing, IEEE Transactions on*, 34(2):331–341, 1986.

[18] Harry B Lee and Michael S Wengrovitz. Resolution threshold of beamspace music for two closely spaced emitters. *Acoustics, Speech and Signal Processing, IEEE Transactions on*, 38(9):1545–1559, 1990.

[19] Steven Thomas Smith. Statistical resolution limits and the complexified crame´ r-rao bound. *Signal Processing, IEEE Transactions on*, 53(5):1597–1609, 2005.

[20] Erdogan Dilaveroglu. Nonmatrix cramér-rao bound expressions for high-resolution frequency estimators. *Signal Processing, IEEE Transactions on*, 46(2):463–474, 1998.

[21] Morteza Shahram and Peyman Milanfar. On the resolvability of sinusoids with nearby frequencies in the presence of noise. *Signal Processing, IEEE Transactions on*, 53(7):2579–2588, 2005.

[22] Inc CVX Research. CVX: Matlab software for disciplined convex programming, version 2.0. `http://cvxr.com/cvx`, August 2012.

[23] Inc Gurobi Optimization. Gurobi optimizer reference manual, 2013.

[24] Petre Stoica and Randolph L Moses. *Introduction to spectral analysis*, volume 1. Prentice hall New Jersey:, 1997.

[25] Richard M Leahy and Brian D Jeffs. On the design of maximally sparse beamforming arrays. *Antennas and Propagation, IEEE Transactions on*, 39(8):1178–1187, 1991.

[26] Ellis L Johnson, George L Nemhauser, and Martin WP Savelsbergh. Progress in linear programming-based algorithms for integer programming: An exposition. *INFORMS Journal on Computing*, 12(1):2–23, 2000.

[27] CW Ang, CM See, and Alex C Kot. Optimization of array geometry for identifiable high resolution parameter estimation in sensor array signal processing. In *Information, Communications and Signal Processing, 1997. ICICS., Proceedings of 1997 International Conference on*, volume 3, pages 1613–1617. IEEE, 1997.

[28] Stephen Poythress Boyd and Lieven Vandenberghe. *Convex optimization*. Cambridge university press, 2004.

[29] Fred Glover. A note on linear programming and integer feasibility. *Operations Research*, 16(6):1212–1216, 1968.

[30] Stephen Bradley, Arnoldo Hax, and Thomas Magnanti. Applied mathematical programming. 1977.

APPENDIX A

PROBABILITY OF AMBIGUITY

Derivations in this part given in [5].

Consider one signal impinging on array of M sensors. Assume that there are two DOA estimation candidates ϕ_1 and ϕ_2. Based on the observations $\{y(k)\}_{k=1}^{K}$, we have to decide whether ϕ_1 or ϕ_2 is the correct DOA.We define the two hypothesis as below.

$$H_1 : \boldsymbol{y}(k) = \boldsymbol{a}(\phi_1)s(k) + \boldsymbol{v}(k) \qquad k = 1, 2, \ldots, K \tag{A.1}$$

$$H_2 : \boldsymbol{y}(k) = \boldsymbol{a}(\phi_2)s(k) + \boldsymbol{v}(k) \qquad k = 1, 2, \ldots, K \tag{A.2}$$

The source signal is denoted by $s(k)$ and noise vector is denoted by $\boldsymbol{v(k)}$. We assume that both noise and source signal are uncorrelated zero-mean Gaussian processes. Let signal variance denoted by $\sigma_s^2 \triangleq E\{s(k)s^*k\}$. Noise covariance is given by $E\{\boldsymbol{n}(k)\boldsymbol{n}(k)^H\} = \sigma^2 \boldsymbol{I}_N$.

Let $\boldsymbol{M_1}$ and $\boldsymbol{M_2}$ denote $Mx1$ mean vectors when H_1 and H_2 is true respectively..

$$\begin{aligned} \boldsymbol{M}_i &= E\{y(k)\} \qquad i = 1, 2 \\ &= \boldsymbol{0}_{NxN} \end{aligned} \tag{A.3}$$

Let $\boldsymbol{R}_1$ and $\boldsymbol{R}_2$ denote NxN covariance matrices when H_1 and H_2 is true respectively.

$$\boldsymbol{R}_i = \sigma_s^2 \mathbf{a}(\phi_i)\mathbf{a}(\phi_i)^H + \sigma^2 \boldsymbol{I}_N \; i = 1, 2 \tag{A.4}$$

The probability density function for a multivariate Gaussian when H_1 is true given by

$$f(\{y(k)\}|\boldsymbol{R}_1) = [(2\pi)^{N/2} \det(\boldsymbol{R}_1)^{\frac{1}{2}}]^{-K} . \exp(-\frac{1}{2}\sum_{k=1}^{K}(\boldsymbol{y} - \boldsymbol{M}_1)^H \boldsymbol{R}_1 (\boldsymbol{y} - \boldsymbol{M}_1)) \tag{A.5}$$

Substituting (A.3) into (A.5), we get

$$f(\{y(k)\}|\boldsymbol{R}_1) = [(2\pi)^{N/2} \det(\boldsymbol{R}_1)^{\frac{1}{2}}]^{-K} . \exp(-\frac{1}{2}\sum_{k=1}^{K}\boldsymbol{y}^H \boldsymbol{R}_1 \boldsymbol{y}) \tag{A.6}$$

Note that $\boldsymbol{x}^H \boldsymbol{R}_1 \boldsymbol{x}$ is just a $1x1$ scalar. So its trace is equal to itself.

$$\begin{aligned} \boldsymbol{y}^H \boldsymbol{R}_1 \boldsymbol{y} &= tr\{\boldsymbol{y}^H \boldsymbol{R}_1 \boldsymbol{y}\} \\ &= tr\{\boldsymbol{y}\boldsymbol{y}^H \boldsymbol{R}_1\} \end{aligned} \tag{A.7}$$

where the cyclic property of trace operator $tr\{\boldsymbol{ABC}\} = tr\{\boldsymbol{CAB}\}$ is used. So (A.6) becomes

$$f(\{y(k)\}|\boldsymbol{R}_1) = [(2\pi)^{N/2} \det(\boldsymbol{R}_1)^{\frac{1}{2}}]^{-K} . \exp(-\frac{1}{2} tr\{\sum_{k=1}^{K} (\boldsymbol{y}\boldsymbol{y}^H)\boldsymbol{R}_1\}) \tag{A.8}$$

Sample covariance matrix is defined as

$$\tilde{R} \triangleq \frac{1}{K} \sum_{k=1}^{K} \boldsymbol{y}\boldsymbol{y}^H \tag{A.9}$$

Substituting (A.9) into (A.8),

$$\begin{aligned} H_1 : f(\{y(k)\}|\boldsymbol{R}_1) &= [(2\pi)^{N/2} \det(\boldsymbol{R}_1)^{\frac{1}{2}}]^{-K} . \exp(-\frac{1}{2} K tr\{\boldsymbol{R}_1^{-1} \tilde{\boldsymbol{R}}\}) \\ H_2 : f(\{y(k)\}|\boldsymbol{R}_2) &= [(2\pi)^{N/2} \det(\boldsymbol{R}_2)^{\frac{1}{2}}]^{-K} . \exp(-\frac{1}{2} K tr\{\boldsymbol{R}_2^{-1} \tilde{\boldsymbol{R}}\}) \end{aligned} \tag{A.10}$$

Assuming that a priori probabilities of H_1 and H_2 are equal, minimum probability of error in choosing between H_1 and H_2 is obtained by the likelihood ratio test.

$$\epsilon \triangleq \frac{f(\{y(k)\}|\boldsymbol{R}_1)}{f(\{y(k)\}|\boldsymbol{R}_1)} \lessgtr 1 \tag{A.11}$$

Substituting the density functions of H_1 and H_2 into (A.11) then taking the ln of both sides we get an equivalent test as below.

$$\begin{aligned} \epsilon &= tr\{(\boldsymbol{R}_1^{-1} - \boldsymbol{R}_2^{-1})\tilde{\boldsymbol{R}}\} \lessgtr 0 \\ &= \frac{1}{K} \sum_{k=1}^{K} \boldsymbol{y}^H (\boldsymbol{R}_1^{-1} - \boldsymbol{R}_2^{-1}) \boldsymbol{y} \lessgtr 0 \end{aligned} \tag{A.12}$$

It can be seen that summation terms in (A.12) are just some random numbers. According to central limit theorem, left hand side of (A.12) will have a normal distribution for large enough snapshots.

Mean values ϵ for both hypothesis are given by

$$\begin{aligned} \mu_1 &= E\{\epsilon|H_1\} \\ &= tr\{\boldsymbol{I}_N - \boldsymbol{R}_2^{-1}\boldsymbol{R}_1\} \end{aligned} \tag{A.13}$$

$$\begin{aligned} \mu_2 &= E\{\epsilon|H_2\} \\ &= tr\{\boldsymbol{R}_1^{-1}\boldsymbol{R}_2 - \boldsymbol{I}_N\} \end{aligned} \tag{A.14}$$

and the variances of ϵ are given by

$$\begin{aligned}\delta_1^2 &= E\{(\epsilon-\mu_1)^2|H_1\} \\ &= \frac{1}{K}tr\{(\boldsymbol{I}_N - \boldsymbol{R}_1^{-1}\boldsymbol{R}_2)^2\}\end{aligned} \tag{A.15}$$

$$\begin{aligned}\delta_2^2 &= E\{(\epsilon-\mu_2)^2|H_2\} \\ &= \frac{1}{K}tr\{(\boldsymbol{R}_1^{-1}\boldsymbol{R}_2 - \boldsymbol{I}_N)^2\}\end{aligned} \tag{A.16}$$

After some algebraic operations mean and variances of ϵ can be simplified as

$$\begin{aligned}\mu_2 &= p[1-\beta^2] \\ \delta_2^2 &= \frac{1}{K}([\mu_2+1]^2-1)\end{aligned} \tag{A.17}$$

where

$$p \triangleq \frac{(\frac{M\sigma_s^2}{\sigma^2})^2}{1+\frac{M\sigma_s^2}{\sigma^2}} \tag{A.18}$$

$$\beta \triangleq \frac{|\boldsymbol{a}(\phi_1)^H\boldsymbol{a}(\phi_2)|}{M} \tag{A.19}$$

Probability of choosing H_1 when H_2 is true is given by

$$\begin{aligned}P_a &= Prob\{\epsilon>0|H_2\} \\ &= \Phi(\frac{\mu_2}{\delta_2})\end{aligned} \tag{A.20}$$

where complementary error function $\Phi(x)$ is given by

$$\Phi(x) \triangleq \frac{1}{2\pi}\int_x^\infty \exp^{-\frac{t^2}{2}}\,dt \tag{A.21}$$

So the ambiguity probability is given by

$$P_a = \Phi\left(\sqrt{\frac{K}{1+\frac{2}{p(1-\beta^2)}}}\right) \tag{A.22}$$

APPENDIX B

ML ESTIMATION FOR SINGLE SOURCE CASE

Consider a scenario where single source signal impinging on an array of M sensors from the direction ϕ_s. Sensor array output is given by

$$\boldsymbol{y}(k) = \boldsymbol{a}(\phi_s)s(k) + \boldsymbol{v}(k) \qquad k = 1, 2, \ldots, K \tag{B.1}$$

where $s(k)$ is assumed to be a deterministic signal and $\boldsymbol{v}(k)$ is both spatially and temporally white Gaussian noise with variance σ_n^2.

The basic idea behind the beamformer technique is to steer the array in one direction at a time and measure the output power of the beamformer. When the steered direction coincides with the DOA, signal coming from each sensor will add up coherently and maximum output power will be observed. Output signal of the beamformer is given by

$$y_F(k) \triangleq \boldsymbol{w}^H \boldsymbol{y}(k) \tag{B.2}$$

where $\boldsymbol{w}$ denotes the weights of the beamformer. For data independent beamformer, weights are chosen as the steering vector normalized with the number of elements.

$$\boldsymbol{w} = \frac{\mathbf{a}(\phi)}{\sqrt{M}} \tag{B.3}$$

Total average output power of the beamformer for steering direction ϕ is given by

$$\begin{aligned} P(\phi) \triangleq \frac{1}{K}\sum_{k=1}^{K} |\boldsymbol{y}_f(k)|^2 &= \frac{1}{K}\sum_{k=1}^{K} \frac{1}{M} |\boldsymbol{a}(\phi)^H \boldsymbol{y}(k)|^2 \\ &= \frac{\boldsymbol{a}(\phi)^H \tilde{\boldsymbol{R}} \boldsymbol{a}(\phi)}{M} \end{aligned} \tag{B.4}$$

where $\tilde{\boldsymbol{R}} \triangleq \frac{1}{K}\sum_{k=1}^{K} \boldsymbol{y}\boldsymbol{y}^H$ denotes the sample covariance matrix.

Now we will show that data independent beamformer and the ML estimation for single source case is essentially the same thing. To do so, we start by writing likelihood function of the observations given in Eq.B.1.

$$f_y(\boldsymbol{y}) = \prod_{k=1}^{K} (\pi\sigma_n^2)^{-M} exp\left[-\frac{||\boldsymbol{y}(k) - \boldsymbol{a}(\phi)s(k)||^2}{\sigma_n^2}\right] \tag{B.5}$$

Negative log likelihood function is given by

$$\ell_{DML} = M\ log(\pi\sigma_n^2) + \frac{1}{\sigma_n^2}\sum_{k=1}^{K} ||\boldsymbol{y}(k) - \boldsymbol{a}(\phi)s(k)||^2 \tag{B.6}$$

When we look into the Eq.B.6, we see that the ML estimate of the DOA can be given by

$$\hat{\phi} = \underset{\phi}{\text{argmin}} \sum_{k=1}^{K} \left\{||\boldsymbol{y}(k) - \boldsymbol{a}(\phi)s(k)||^2\right\} \tag{B.7}$$

After some algebraic operations and using the properties of the $tr\{\}$ operator, ML estimate can be written as

$$\hat{\phi} = \underset{\phi}{\text{argmin}}\ tr\left\{\boldsymbol{\Pi}_A^{\perp}\tilde{\boldsymbol{R}}\right\} \tag{B.8}$$

where $\tilde{\boldsymbol{R}}$ is the sample covariance matrix and $\boldsymbol{\Pi}_A^{\perp}$ is the orthogonal projector on to the noise subspace given by

$$\begin{aligned} \boldsymbol{\Pi}_A^{\perp} &\triangleq \boldsymbol{I} - \mathbf{a}(\phi)[\mathbf{a}^H(\phi)\mathbf{a}(\phi)]^{-1}\mathbf{a}^H(\phi) \\ &= I - \frac{\mathbf{a}(\phi)\mathbf{a}^H(\phi)}{M} \end{aligned} \tag{B.9}$$

Substituting the Eq.B.9 into the Eq.B.8 we get,

$$\hat{\phi} = \underset{\phi}{\text{argmax}}\ tr\left\{\mathbf{a}(\phi)\mathbf{a}^H(\phi)\tilde{\boldsymbol{R}}\right\} \tag{B.10}$$

By using the cyclic property of trace operator ($tr\{\boldsymbol{ABC}\} = tr\{\boldsymbol{BCA}\}$) we can write the Eq.B.10 as

$$\hat{\phi} = \underset{\phi}{\text{argmax}}\ tr\left\{\mathbf{a}^H(\phi)\tilde{\boldsymbol{R}}\mathbf{a}(\phi)\right\} \tag{B.11}$$

Note that the function inside trace operator in Eq.B.11 is a scalar and it is the output power of the beamformer given in Eq.B.2. So for single source case, ML estimation is equivalent to the data independent beamformer.